Gamma ray signals from annihilating dark matter in curved spacetime

by

Trond Fredheim

Thesis

for the degree of

Master of Science

Faculty of Mathematics and Natural Sciences
University of Oslo

May 15, 2016

Abstract

In order to investigate gamma ray signals from dark matter originating from close to the black hole at the galactic center, we investigate the effects of general relativity on such a signal. The expression for the photon flux in flat spacetime is derived, and then generalized to take into account the geodesics of the photons, as well as the gravitational redshift. We calculate $J(\psi)$ in the Schwarzschild spacetime, and find the photon flux for the case where the particles annihilate at rest. It is found that these relativistic considerations could potentially alter the spatial signal, but mostly for angular resolutions too small for present day detectors, and only in a region heavily influenced by uncertainties in the dark matter halo. The spectral signal shows a redshift of $\Delta x = 0.1$, which should in principle be detectable if we had a better understanding of the background processes. The spectrum also shows potential features for smaller x, though these features might be because of numerical errors.

Acknowledgements

A big thanks goes to my supervisor Torsten Bringmann, for providing me with such an interesting and challenging subject for my thesis and for sharing with me some of his vast knowledge of physics. I would also like to thank my family, for always being supportive and for their interest in my studies and my well-being.

In addition, I want to thank all the employees at the theoretical physics group, as well as my fellow master students. Their friendliness always made me feel welcome, and I always looked forward to the entertaining lunch time conversations.

Finally, I especially want to thank Ida Pauline Buran for being such a great friend through all my years at UiO, for countless cups of tea and waffles, and for the good company.

Contents

Chapter 1

Introduction and outline

Today there is solid evidence for the existence of a substantial dark matter (DM) component in the universe. Recent data from the Planck collaboration gives a physical DM density of $\Omega_\chi h^2 = 0.1188 \pm 0.0010$, where h is the reduced Hubble constant defined by $H_0 = 100h$ km/s/Mpc $= 67.74 \pm 0.46$ km/s/Mpc [1]. This means that DM makes up $\sim 25\%$ of the total energy density of the universe. However, the nature of this elusive matter remains unknown. Out of the many proposed solutions, the possibility of Weakly Interacting Massive Particles (WIMPs) is one of the most appealing, since they seem to satisfy all the criteria of DM from a wide range of different observations [2]. For example, the DM annihilation cross section which produces the correct relic density is just the cross section one would expect for a particle interacting though the weak force, which also allows the particle to be massive enough not to have been detected by collider experiments [3]. The weak interaction of WIMPs also means that their relic density today is a result of thermal production in the early universe. The detection of these particles, either directly or indirectly, is crucial for determining what DM is and for settling a debate which is undoubtedly one of the most important unsolved mysteries in physics.

In order to make up the majority of matter in the universe today, the DM particle has to be stable. But since they are weakly interacting, they can annihilate to produce standard model (SM) particles. This gives us an indirect method for detecting DM non-gravitationally. Out of the many produced particles, photons are of particular interest, as they can propagate mainly undisturbed through the galaxy and therefore point directly to their source. One promising place to look for gamma rays from DM is at the center of the Milky Way galaxy, where the DM density is expected to be especially high. But we know that for the photons coming from the very center of our galaxy, they have to come close to a supermassive black hole. It is therefore of interest to calculate the effects of the theory of general relativity on these photons, as they should at some radius begin to be influenced by the extreme gravitational field of the black hole.

When performing calculations involving DM annihilations in the galaxy, it

is usually assumed that the DM particles annihilate at rest, i.e. with vanishing relative velocity. However, when the DM particles annihilate in the vicinity of the black hole, it is reasonable to assume that the relative velocity of the particles can no longer be neglected. In fact, in may be the case that the black hole can act as a particle accelerator for DM, producing energies of several times the rest mass [4].

One DM model of particular interest is the Kaluza-Klein (KK) model, where spacetime is assumed to consist of one or several extra spatial dimensions through which all SM fields can propagate. In this case, the momentum of particles in these curled up, extra dimensions (ED) are observed as additional mass states in the effective 4-dimensional theory. Some of these new particles provide excellent candidates for DM [5]. If this is the case, then when the full velocity dependence is taken into account when calculating gamma ray spectra the signal can provide striking features, in the best case scenario producing a comblike structure of gamma ray lines as shown in [6]. In that article, the effects of gravitational and Doppler redshift have also been described. However, it seems no investigation of other general relativistic effects have been done.

Our goal is therefore to investigate the effect of some of the features in general relativity on the gamma ray signal from DM, specifically to take into account the curved photon geodesics and the gravitational redshift for photons in the vicinity of a black hole.

The outline of this thesis is as follows: In chapter 2, a brief introduction to the subject of DM is given, with some history and the general features of WIMPs. we also include a summary of the different methods of detection, with a main focus on indirect gamma ray detection. We then present some popular choices of DM halo profiles, with special attention to the profile close to a black hole.

In chapter 3 the general properties of KK theories are presented, with emphesis on the case of one ED. We briefly present the model of universal extra dimensions, as well as the basic features of KK DM.

In chapter 4 we focus on the gamma ray signal from DM, briefly considering the different annihilation channels that produce photons. We then derive the expression for the photon flux in flat spacetime, and apply this to a simple example in our galaxy before generalizing the expression to take into account some effects of general relativity, using the Schwarzschild spacetime as our example.

In chapter 5, we apply this generalized expression to our galaxy and state our results.

Chapter 2

Introduction to dark matter

The first suggestion of a non-luminous gravitational contribution is usually attributed to Fritz Zwicky's observations of the Coma cluster from 1933 [7], and it was also Zwicky who coined the term *dark matter*. Zwicky used the Doppler shift of light from galaxy clusters to find the velocities of galaxies within the cluster, and compared this to the velocity distribution he expected from using the virial theorem on the mass inferred from the luminous matter. He found that the galaxies were moving much too fast for the cluster to be gravitationally bound, and concluded that most of the cluster had to consist of non-luminous matter. Although Zwicky slightly overestimated the ratio of dark to luminous matter in the Coma cluster by using too large a value for the Hubble parameter, his conclusion was still correct and his result still stands as one of the first evidences for DM.

Even though the concept of DM had been around since the 1930s, it wasn't until the 1970 that the idea began to be taken seriously, when Vera Rubin and others studied the rotation curve of stars in the Andromeda galaxy and found that the orbital velocities of the stars as a function of the radius seemed to remain constant, instead of dropping quickly as one would expect from the amount of inferred mass in the galaxy [8]. Afterwards the rotation curves of several other galaxies were found, and they all showed that there should be more matter present than what the stars and gas could account for.

There is also evidence for DM on larger scales, using gravitational lensing of light around galaxy clusters. The light from objects behind the cluster is deflected as it passes by, sometimes producing several images of the same object as viewed from earth. The distortion of light around galaxy clusters can be used to find the total gravitational mass, while one can use optical methods to determine the luminous mass. Any difference between the two measurements must then be caused by DM. One particularly interesting cluster is the so-called *Bullet Cluster*, which consists of two different clusters that recently collided [9]. In this case the gas clouds in the clusters have slowed down after the collision due to electromagnetic interactions, and since this gas makes up most of the

luminous matter of the cluster, one would expect most of the total mass to lie in the same area as the gas. However, gravitational lensing shows that most of the mass approximately follows the galaxies of the cluster, which have passed straight through each other without interacting. This means that a large part of the cluster must be made up of DM which does not interact strongly with itself. The bound on the self-interaction cross section of DM in the Bullet Cluster obtained from measurements is $\sigma/m < 0.7\,\mathrm{cm}^2\mathrm{g}^{-1}$ [10], which almost completely excludes the allowed range for theories with self-interacting DM, which requires σ/m to be in the range $0.5 - 6\,\mathrm{cm}^2\mathrm{g}^{-1}$ in order to explain the flat inner mass profils of galaxies [11]. Thus the Bullet Cluster shows us that not only evidence of a significant amount of DM, but also that this DM must be weakly interacting, if it interacts at all.

One of the most important pieces of evidence for DM comes from the Cosmic Microwave Background (CMB). This is the leftover radiation from the early universe, when the temperature had dropped enough that the plasma of ionized baryons and electrons recombined into neutral atoms. This made the universe transparent to radiation, since photons could now travel through it without scattering on charged particles. The CMB thus provides us with a snapshot of the universe at this excact moment of so-called recombination. While this radiation is extremely uniform and isotropic, the small temperature fluctuations of the CMB contains invaluable information about the structure of the universe at early times, since these fluctuations reflect the structure of the ionized plasma which would later collapse to form galaxies. If the matter content of the early universe was mostly dark, one should then be able to see its effect on the CMB today. The CMB has been mapped by the WMAP and more recently the Planck experiment, who have used the data to determine several cosmological parameters, including the total amount of dark and baryonic matter in the universe. They concluded that the DM density is $\Omega_\chi h^2 = 0.1188 \pm 0.0010$, while the baryonic matter density is $\Omega_b h^2 = 0.02230 \pm 0.00014$, where h is the reduced Hubble constant, $H_0 = 100h\,\mathrm{km/s/Mpc}$ [1]. Thus there is over five times as much DM as there is ordinary matter.

Since all the evidence we have for DM is in some sense gravitational, attempts have been made to explain the observations by assuming that our current theory of gravity, General Relativity, is not valid at all scales. One well known example of such a theory is Modified Newtonian Dynamics (MOND) [12], which proposes a different gravitational force law for the stars closer to the edge of the galaxy, but so far all such theories seem to be unable to explain all independent DM observations at the same time. It therefore seems tempting to assume that DM is some new type of particle with properties that has so far made it impossible to detect by means other than gravitational, such as a weak interaction with electromagnetism. By determining the properties such a particle must have, scientists have come up with a type of particles able to explain all the DM

observations at once, which is the topic of the next section. Because of this, the general consensus today is that DM is in fact a new type of matter.

2.1 The WIMP paradigm

In this section, we will discuss some of the properties of the DM candidates known as WIMPs. For a more detailed analysis, see e.g. [3].

The standard model of particle physics is arguably the most successful particle physics theory to date. However, there are several problems that the SM is not able to solve, for example the *hierarchy problem*. In short, this is the problem of why the Higgs particle has the low (compared to the Planck scale) mass that it has, when one takes into consideration mass corrections from loop diagrams. These corrections should make the Higgs mass explode, unless there is a large amount of fine-tuning to make the mass corrections cancel each other out. This can be done in a more natural way by introducing new particles to the theory which couple to the Higgs, as is done for example in the theory of supersymmetry (SUSY).

There are several proposed extensions to the standard model which predict new, exotic particles. If the theory in addition contains a new conserved symmetry obeyed by these particles, then the lightest of them must be stable, unable to decay to lighter SM particles. Examples of this include the R-parity of SUSY and the KK-parity of universal extra dimensions (UED). If this stable particle interacts with SM particles only through a force with similar strength as the weak nuclear force and has a mass in the GeV – TeV range, it satisfies the conditions of a WIMP.

The amount of DM in the universe today is determined by its interactions with SM particles in the early universe, with DM particles annihilating into SM particles and vice versa. The evolution of the number density n_χ is described by the Boltzmann equation,

$$\frac{dn_\chi}{dt} = -3Hn_\chi - \langle\sigma v\rangle(n_\chi^2 - n_{eq}^2), \tag{2.1}$$

where $H = \dot{a}/a$ is the Hubble expansion rate of the universe, $\langle\sigma v\rangle$ is the thermally averaged DM annihilation cross section times the relative velocity of the DM particles and n_{eq} is the number density in thermal equilibrium. The first term describes the decrease in density due to the expansion of the universe, while the second term describes changes due to deviations from the equilibrium density.

In the early universe, the first term is small and can be ignored, which means that any change in the DM density would be driven back to equilibrium, causing the density to drop as $e^{-m/T}$. This behaviour continues until the expansion term becomes large, and eventually the second term can be ignored, giving the equation

$$\frac{dn_\chi}{dt} + 3Hn_\chi = 0. \tag{2.2}$$

when using that $H = \dot{a}/a$ and multiplying both sides with a^3, we can write this as

$$\frac{d}{dt}(a^3 n_\chi) = 0, \tag{2.3}$$

which means that the DM density in a comoving volume of space $a^3 n_\chi$, called the *comoving density*, becomes constant as the universe becomes colder. This process is usually referred to as "freeze out", and is illustrated in figure 2.1 which shows the time and temperature evolution of the comoving DM number density. The value at which the freeze out happens depends on the annihilation cross section of DM, as a higher cross section means it will take longer for the expansion term to take over and thus for the comoving density to stabilize.

The process can be thought of more heuristically as follows: the DM particles are in equilibrium with the SM particles in the early universe, with both DM and SM particles annihilating into each other at equal rates. But as the universe expands, the average temerature of the SM particles is no longer high enough to produce DM, while the DM annihilation is still unaffected, and the DM density drops exponentially. At some point however, the expansion rate is so high that the DM particles become to diluted to annihilate efficiently and the density stabilizes, giving the DM density we observe today.

The present DM density can be calculated to be [3]

$$\Omega_\chi h^2 = 0.1 \times \frac{3 \times 10^{-26}\text{cm}^3/\text{s}}{\langle \sigma v \rangle}, \tag{2.4}$$

which means that particles with interactions and masses around the weak scale have just the right annihilation cross section to account for the DM we observe today, since

$$\langle \sigma v \rangle \sim \frac{\alpha_{weak}^2}{m_{weak}^2} \sim 10^{-25}\text{cm}^3/\text{s}. \tag{2.5}$$

This is called the *WIMP miracle*.

It is important to stress that WIMPs were not introduced to solve the DM problem specifically. Instead, they are a natural consequence of theories that try to solve the problems of the SM, such as the hierarchy problem. This is one of the main reasons why the WIMP solution to DM is so appealing.

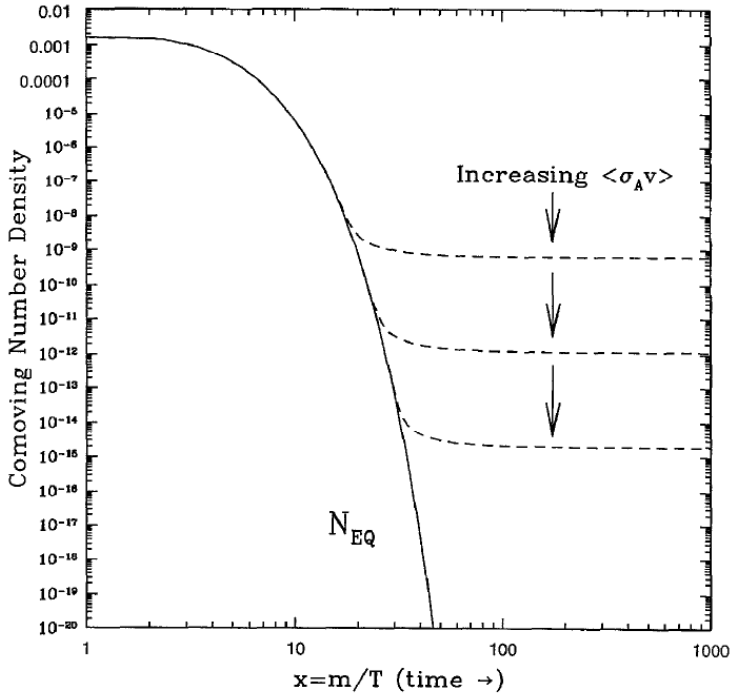

Figure 2.1: The comoving number density of DM as the universe cools with time. The solid line is the equilibrium solution, where the DM density drops exponentially. When the expansion of the universe begins to dominate, the particles can no longer annihilate efficiently, and the density only drops as $1/a^3$, meaning the comoving density becomes constant and the DM "freezes out". The value at which the freeze out happens depends on the annihilation cross section, with a higher cross section meaning a lower freeze out value. Figure from [3].

2.2 Methods of detection

Searches for DM can be categorized into three main categories: production of DM at particle colliders, direct detection of DM elastically scattering with SM particles, and indirect detection of the SM decay or annihilation products of DM. We here give a brief overview of the different detection methods, with a main focus on indirect detection of gamma rays. For a thorough review, see [13].

2.2.1 Particle colliders

If DM is a particle with mass around 100 GeV, it should be possible to detect at present day colliders. Since DM interacts so weakly with SM particles, it would simply leave the detector in the form of missing transverse energy. In the case of DM pair production one might then naively think DM would be undetectable,

since both particles would escape the detector without a trace. But if one of the initial particles radiates a SM particle, for example a gluon at a hadron collider, then this particle would leave a signal in the detector and there would be an energy imbalance due to the missing DM particles. At a hadron collider like the LHC, initial state radiation of a gluon would cause a single hadron jet, and searching for these monojets and missing transverse energy is one of the methods used to look for DM.

It is also possible to produce DM through more complicated processes, where the particle initially produced in the collider is some other, more massive new exotic particle. This particle would be highly unstable, and would quickly decay to lighter particles, both exotic and SM ones. The SM decay products would be registered by the detector, but the exotic particles would continue to decay until the only exotic particle left is the lightest and stable particle. This is the DM particle, but as it has very weak interactions with ordinary matter it would simply leave the detector without a trace, only showing up as missing total energy when the SM decay products are added up. This information could then be used to set limits on the properties of DM. These decay cascades are usually very model dependent however, which makes it difficult to use them to set bounds on the DM scattering cross section.

2.2.2 Direct detection

Direct detection experiments attemt to measure the interaction of DM particles with SM nuclei in low background scattering experiments. The scattering rate per recoil energy can be written [14]

$$\frac{dR}{dE_R} = \frac{\rho_0}{m_N m_\chi} \int_{v_{\min}}^{v_{\text{esc}}} v f(v) \frac{d\sigma}{dE_R} \, dv, \tag{2.6}$$

where ρ_0 is the DM halo density at the position of the earth, M_N is the mass of the target nucleus and m_χ is the mass of the DM particle. $d\sigma/dE_R$ is the differential scattering cross section, and $f(v)$ is the velocity distribution of the DM halo. The integral is taken over all possible velocities, from the lowest DM velocity $v_{\min}$ which can give the nucleus a recoil energy to the velocity where the DM particles can escape from the halo, v_{esc}.

The scattering cross section can be calculated in any given DM model, while the galactic halo density and velocity distribution must be calculated from other methods and are subject to large uncertainties. Since the scattering cross section for DM is very low, direct detection experiments need to be almost completely free of background events in order to see a DM signal. To achieve this, the detectors are usually placed deep underground to shield them from cosmic rays. Another strategy for direct detection is to look for an annual modulation of the signal, which should be caused by the earth's changing velocity relative to the

DM halo as it moves around the sun. Unfortunately, results from direct detection experiments are inconclusive and in some cases even in conflict with each other. The DAMA/LIBRA experiment sees an annual modulation of their signal [15], but this result disagrees with other similar experiments.

2.2.3 Indirect detection

Indirect detection experiments attempt to measure the SM end products of annihilating or decaying DM in the form of cosmic rays. There are several different end products which in principle can be detected, all with different advantages and drawbacks.

Photons

Photons are perhaps the most obvious form of cosmic rays for detecting DM. They have the clear advantage of travelling in straight lines from the source to the observer, which means that they carry both spectral and spatial information about their origin. If the photons are produced directly from the annihilation, for example through the processes $\chi\chi \to \gamma\gamma$ or $\chi\chi \to Z\gamma$, then the energy spectrum would contain a sharp line or cutoff, respectively, located exactly at the DM mass. The majority of photons are usually produced through other processes however, such as the decay products of other SM final states (mostly pions) or synchrotron radiation from charged particles due to magnetic fields in the galaxy. Such processes produce broader, smeared out spectra, and are more difficult to use to detect DM.

The main challenge with using photons for indirect detection is the large backgrounds. There are several sources of gamma rays in the galaxy, such as pulsars and supernova remnants, and also other sources which are not completely understood. This makes some of the gamma rays from DM difficult to distinguish from the background, since they produce broad bumps with no distinct spectral signature. However, the monochromatic lines produced by direct annihilation into photons can in some DM models be significant enough that it becomes possible to seperate the signal from the background. In general this is not the case though, and higher resolution detectors are needed to be able to see a signal.

The expected differential photon flux per energy from annihilating DM in a direction ψ is given by

$$\frac{d\Phi_\gamma}{d\Omega dE_\gamma}(E_\gamma, \psi) = \frac{1}{8\pi} \int_{\text{l.o.s.}} dl(\psi) \rho_\chi^2(\mathbf{r}) \left[\frac{\langle \sigma v \rangle}{m_\chi^2} \sum B_f \frac{dN_\gamma^f}{dE_\gamma} \right], \tag{2.7}$$

where l.o.s. means taking the integral along the line of sight, ρ_χ is the DM halo density, $\langle \sigma v \rangle$ is the velocity-weighed annihilation cross section and m_χ is the mass of the DM particle. B_f is the branching ratio into channel f and N_f is

the number of photons produced per annihilation. The flux is averaged over the opening angle of the detector, $\Delta\psi$. If the DM particle is not its own antiparticle, the expression changes by a factor 1/2. This expression is deduced in chapter 4.1.

As can be seen from the expression, the flux is dependent on the square of the DM halo density. This means that the result is highly sensitive to the details of the halo, which is largly unknown and subject to much uncertainty. But the square dependence also means that it's favourable to look for DM in regions of high DM density, such as the center of the Milky Way. The dwarf galaxies surrounding our own are also prime targets for searching for DM, as they are believed to have large DM halos relative to their luminous mass, meaning there should be less background and therefore easier to distinguish a DM signal.

There have been a few claims of indirect DM detection. In 2012, it was discovered that the data from the Fermi Large Area Telescope contained a line at ~ 130 GeV, coming from the galactic center [16]. This has been attempted to explain as a DM signal by many, but it is still entirely possible that the signal is due to other sources, and the significance also seems to have diminished with more data, making it more likely to be a statistical accident [17].

Neutrinos

Neutrinos are also a method of indirect detection, and they are in many ways similar to photons, since they also point directly to the source. The backgrounds for neutrinos are smaller than for photons, but neutrinos are much more difficult to detect. Still, there are detectors dedicated to measuring them, both from astrophysical sources and from processes in the sun. One thing that is unique for neutrinos is that they can be used to detect DM trapped in the Sun or the Earth. As DM particles travels through baryonic matter, there is a small chance that they will scatter and lose energy, which can cause them to become trapped in the gravitational field of the Sun or the Earth. There they will build up and eventually annihilate with each other, producing SM particles. Of these particles, only neutrinos can escape without interacting, which means they are the only result of this process which potentially can be detected here on Earth. The IceCube detector located at the geografical south pole is one of the most recent neutrino detectors, and has set limits on the annihilation cross section of DM in the Sun [18].

Antimatter

Charged particles in general have the disadvantage that they are affected by the magnetic fields of the galaxy, since the inhomogeneities of the fields cause them to scatter and change direction. The particles therefore lose their directional information, and their propagation must be modeled as a diffusive process. One

therefore has to rely mainly on the energy spectrum alone to search for DM. Because there is so much more matter than antimatter in the universe, the background for antimatter is much smaller. And since both matter and antimatter are assumed to be created in equal amounts from DM annihilation, there is a clear advantage to using antiparticles to detect DM. The PAMELA experiment discovered in 2009 a definite excess of high energy positrons [19], which has later been confirmed by other experiments. If this was due to DM however, one would in most models also expect an excess of antiprotons from DM decaying into quarks, and this is not seen by any experiments. Therefore, it is likely that the positron excess is due to other astrophysical sources.

2.3 Halo profiles

We here give a short description of different DM profiles, with additional focus on the profile in the vicinity of a black hole. For a more detailed review, see for example [20].

2.3.1 A general parametrization

As we have seen, the exact density profile of the DM halo is of great importance if one wishes to detect DM. Unfortunately, direct observation of our galaxy cannot adequately constrain the shape of the halo, and so we must turn to other means. Most DM halo profiles are results of N-body computer simulations of galaxy formations with cold dark matter. A parametrization which covers several of these, is given by

$$\rho(r) = \rho_0 \left(\frac{R_0}{r}\right)^{\gamma} \left[\frac{1 + (R_0/r_s)^{\alpha}}{1 + (r/r_s)^{\alpha}}\right]^{\frac{\beta-\gamma}{\alpha}}, \tag{2.8}$$

where α, β and γ are the parameters which specify the profile. $\rho_0 \simeq 0.4\,\mathrm{GeV/cm^3}$ is the DM density at the position of the Sun [21], $R_0 \simeq 8.5$ kpc is the distance from the Sun to the galactic center, and r_s is a scale radius which determines when the profile changes from depending on $r^{-\beta}$ for large r to depending on $r^{-\gamma}$ for small r. A much used profile is the Navarro-Frenk-White (NFW) profile [22], with $(\alpha, \beta, \gamma) = (1, 3, 1)$ and $r_s \simeq 20$ kpc.

These models which are favoured from computer simulations all exhibit similar behaviour at small r, namely that the density increases steeply for smaller distances, usually called *cusps*. However, observations of rotation curves from satellite galaxies of the Milky Way suggest that the profile flattens out for small r, so-called *cores*. This disagreement between simulations and observations of smaller galaxies is called the *core-cusp problem*. This problem is still unsolved, with possible solutions that there is some mechanism that "cores" the halos of

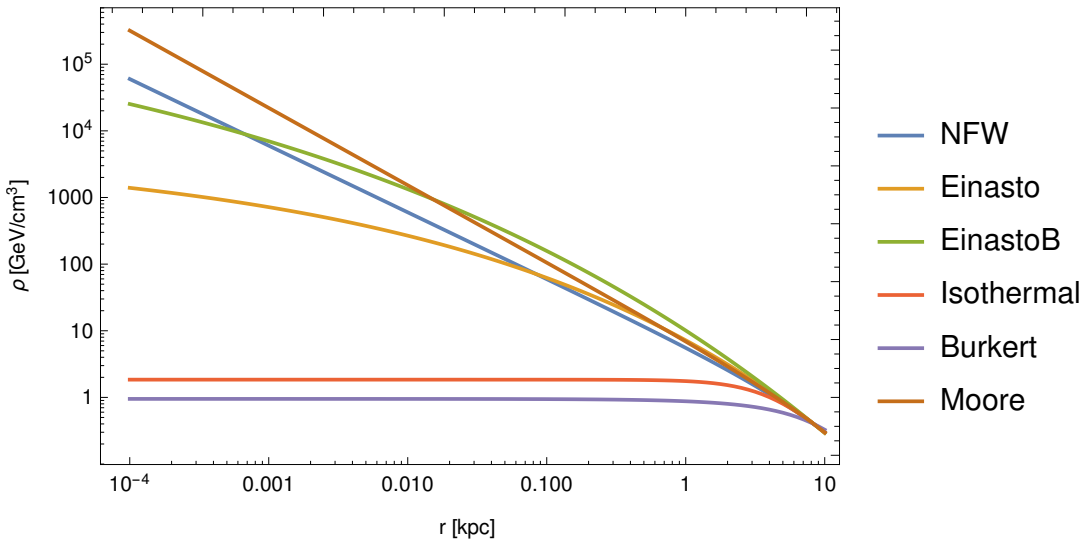

Figure 2.2: Models of DM density profiles for the Milky Way galaxy, using the parameters from [25]. At the position of the Sun, all profiles have the same value, but they differ greatly at the inner parts of the galaxy. The profiles which keep increasing for smaller r are called *cuspy* profiles, while the ones which flatten out and become constant are called *cored*.

the dwarf galaxies, for example *baryonic feedback*, where some mechanism drives baryonic matter out of the central regions which can be shown to "core" the halo profile [23]. Another possibility is that the assumption of cold DM is simply wrong, and that some other type of DM would provide cored profiles also in larger galaxies. In addition, since all simulations of galaxy formation have some smallest resolution the innermost part of the halo has to be inferred by extrapolation, and is therefore bound to be more uncertain than the rest of the halo.

Another type of halo profile which is preferred by more recent simulations is the Einasto profile [24],

$$\rho(r) = \rho_0 \exp\left(-Ar^\alpha\right), \tag{2.9}$$

where α determines the degree of curvature of the profile.

Figure 2.2 shows some of the most common Milky Way halo profiles used in computations, with parameters taken from [25]. For indirect detection of DM from the galactic center, the innermost part of the halo is of great importance, since the flux depends on the square of the DM density, as we have seen. The best case scenario for indirect detection would therefore be a cuspy profile such as the NFW profile, in order to pick out the signal from the background.

2.3.2 The profile close to a black hole

Even though these density profiles fit nicely with observations on larger scales such as rotation curves, the innermost regions are subject to influences from the baryonic matter of stars and gas, in addition to the supermassive black hole at the center. It is therefore possible that the halo looks significantly different inside the central parsec of the galaxy. If the black hole was formed from a slow accretion of gas, It could create a density spike in the DM halo [26]. Although processes such as DM annihilations and DM interaction with stars could reduce these spikes [27], there still could be a significant difference from a straight forward NFW profile. As we get closer to the black hole however, the density eventually gets high enough that DM annihilations become important over the lifetime of the black hole, causing the density to stabilize and form a plateau at a radius r_p where the annihilation time equals the age of the black hole [26], $t_{BH} \sim 10^{10}$ years:

$$\rho(r_p)\langle\sigma v\rangle = \frac{m_\chi}{t_{BH}}. \tag{2.10}$$

For our purposes, we will use the profile described in [28],

$$\rho(r) = \begin{cases} \rho_0 \left(\frac{r}{r_{BH}}\right)^{-\gamma'} & r_p < r \leq r_{BH} \\ \rho_0 \left(\frac{r}{r_{BH}}\right)^{-\gamma} & r_{BH} \leq r \end{cases}, \tag{2.11}$$

where $r_{BH} = 2$ pc is the radius of influence of the black hole, $\gamma' = 3/2$ and $r_p = 10^{-5}$ pc. The constant ρ_0 is determined by extrapolating a NFW profile inward, and demanding that the profiles are equal at $r = r_{BH}$.

Figure 2.3 shows the density profile for three different values of γ'. When $\gamma' = 1$ the curve is just a continuation of the NFW profile, while for other values it becomes a broken power law. All three curves stabilize at the density plateau, even though the values for $\gamma' = 1$ are too small to show in the figure.

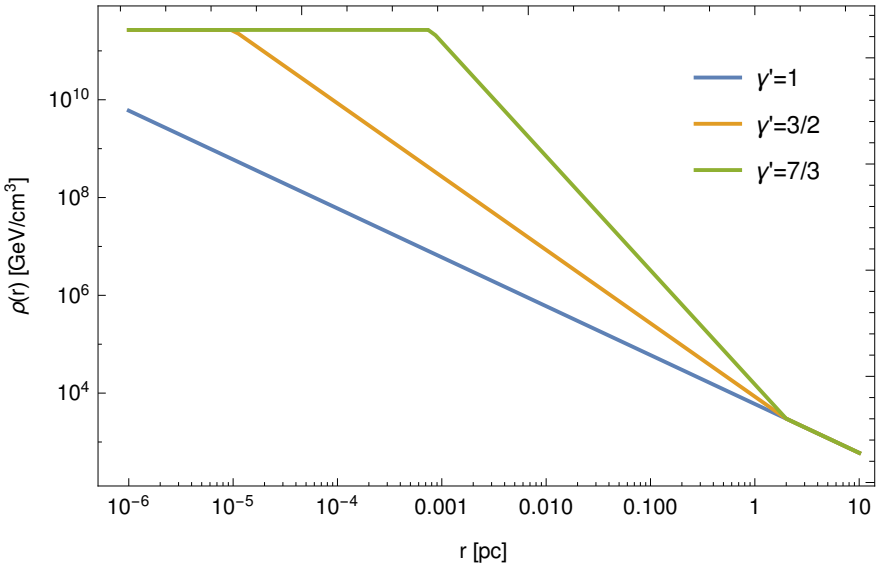

Figure 2.3: The DM density profile close to a black hole where the profile is a broken power law, $\rho^{-\gamma}$ where $\gamma \to \gamma'$ inside the black hole radius of influence, with three different values of γ'. The density plateaus at a radius r_p where the annihilation time equals the age of the black hole. The lowest curve with $\gamma' = 1$ is simply a continuation of the NFW profile, while the others show the profiles for $\gamma' = 3/2$ and $\gamma' = 7/3$, where the latter is the most optimistic case. Although it's not seen in the figure, the profile for $\gamma' = 1$ also stabilizes at the density plateau.

Chapter 3

Introduction to Kaluza-Klein theories

In this chapter, we give a brief introduction to some of the general concepts in Kaluza-Klein theories, as well as some of the history behind it. We then look in some more detail at the theory of universal extra dimensions, giving a brief description of the field content for the case of one extra dimension. A description of the basic ideas from a general relativity perspective can be found in [29], while for a complete description of the particle content in universal extra dimensions, see [30].

3.1 Kaluza's theory

In Einstein's theory of general relativity, the dimensions of space and time are unified into four-dimensional spacetime. In the wake of the success of Einstein's theory in the 1920's, Theodor Kaluza entertained the idea of expanding spacetime by including an additional spatial dimension [31]. His procedure was to introduce a five-dimensional metric $\hat{g}_{MN}$ with $M, N = 0, 1, 2, 3, 4$, which obeyed the five-dimensional Einstein equations in empty space,

$$\hat{R}_{MN} - \frac{1}{2}\hat{R}\,\hat{g}_{MN} = 0, \tag{3.1}$$

where $\hat{R}_{MN}$ is the Ricci tensor in five dimensions and $\hat{R} = \hat{g}_{MN}\hat{R}^{MN}$ is the Ricci scalar. The metric could then be parametrized as follows:

$$\hat{g}_{MN} = \begin{pmatrix} g_{\mu\nu} + \kappa^2\phi^2 A_\mu A_\nu & \kappa\phi^2 A_\mu \\ \kappa\phi^2 A_\nu & \phi^2 \end{pmatrix}, \tag{3.2}$$

where $g_{\mu\nu}$ is the standard four-dimensional metric, A_μ is a tensor field and ϕ is a scalar. κ is a scaling factor for the tensor field. The Ricci tensor and Christoffel symbols in five dimensions are defined the same way as in four dimensions:

$$\hat{R}_{MN} = \partial_A \hat{\Gamma}^A_{MN} - \partial_N \hat{\Gamma}^A_{MA} + \hat{\Gamma}^A_{MN}\hat{\Gamma}^B_{AB} - \hat{\Gamma}^A_{MB}\hat{\Gamma}^B_{AN}, \tag{3.3}$$

$$\hat{\Gamma}^A_{MN} = \frac{1}{2}\hat{g}^{AB}(\partial_M \hat{g}_{BN} + \partial_N \hat{g}_{BM} - \partial_B \hat{g}_{MN}). \tag{3.4}$$

Kaluza assumed what is called the *cylinder condition*, namely that the metric does not depend on the fifth coordinate x^4, so that all derivatives with respect to this coordinate vanishes.

Thus, by inserting (3.4) and (3.3) into the Einstein equation (3.1) or equivalently $\hat{R}_{MN} = 0$, the components $\mu\nu$, $\mu 4$ and 44 eventually give the equations

$$R_{\mu\nu} - \frac{1}{2}Rg_{\mu\nu} = \frac{\kappa^2\phi^2}{2}T^{\mathrm{EM}}_{\mu\nu} - \frac{1}{\phi}[\nabla_\mu(\partial_\nu\phi) - g_{\mu\nu}\Box\phi], \tag{3.5}$$

$$\nabla^\mu F_{\mu\nu} = -3\frac{\partial^\mu\phi}{\phi}F_{\mu\nu}, \tag{3.6}$$

$$\Box\phi = \frac{\kappa^2\phi^3}{4}F_{\mu\nu}F^{\mu\nu}, \tag{3.7}$$

where $T^{\mathrm{EM}}_{\mu\nu} = g_{\mu\nu}F_{\alpha\beta}F^{\alpha\beta}/4 - F^\alpha_\mu F_{\nu\alpha}$, $F_{\mu\nu} = \partial_\mu A_\nu - \partial_\nu A_\mu$, $\Box = \nabla^\mu\nabla_\mu$ and ∇_μ is the four-dimensional covariant derivative.

If one then sets the scalar field to be constant, equations (3.5) and (3.6) become Einstein's field equations and Maxwell's equations in four dimensions. The form of the stress-energy tensor in equation (3.5) is precisely the form of the electromagnetic stress-energy tensor. This means that the vector field A_μ in the metric can be identified as the usual electromagnetic potential. We have thus recovered general relativity and electromagnetism from a unified theory in five-dimensional empty spacetime! The fact that equation (3.7) also puts an additional constraint on the electromagnetic field tensor was not realized by Kaluza and Klein at the time. It was discovered 20 years later, by Jordan [32].

Alternatively, the same result can be achieved by using variational calculus by starting with the Einstein-Hilbert action in five dimensions,

$$S = \frac{1}{16\pi\hat{G}}\int \hat{R}\sqrt{-g}\, d^4x\, dy, \tag{3.8}$$

where $\hat{G}$ is a constant, g is the determinant of the five-dimensional metric and $y = x^4$ is the fifth coordinate. Using the cylinder condition the integral over y can then be pulled outside the integral, and by inserting the metric (3.2), one gets the action

$$S = \int d^4x\sqrt{-g}\phi\left(\frac{R}{16\pi G} + \frac{1}{4}\phi^2 F_{\mu\nu}F^{\mu\nu} + \frac{2}{3\kappa^2}\frac{\partial^\mu\phi\partial_\mu\phi}{\phi^2}\right), \tag{3.9}$$

where $G = \hat{G}/\int dy$. This is the action for general relativity and electromagnetism scaled by the field ϕ, as well as the action for a massless scalar field.

3.2 Compactification

One of Oscar Klein's contributions to Kaluza's theory was to give an explanation for the cylinder condition, by suggesting that the extra dimension was curled up into a circle, with a radius small enough that it was unobservable for our experiments [33]. Particles would then also travel in the direction of the extra dimension, but would move around the circle and almost immediately return to where they started. As a consequence, such a theory would contain additional particles. To understand this, one simply has to realize that while any momentum a particle has in the curled-up dimension would be unobservable to us, we would still measure the extra kinetic energy of this particle. Since this extra energy would not be interpreted as momentum to a four-dimensional oberver, it has to be a particle of larger mass in the four-dimensional theory.

To see this in more detail, let us consider a scalar field ϕ with mass m in five dimensions. Such a field would obey the five-dimensional Klein-Gordon equation,

$$(\partial_{(5)}^2 + m^2)\,\phi(x^\mu, y) = (\partial_t^2 - \nabla^2 - \partial_y^2 + m^2)\,\phi(x^\mu, y) = 0, \tag{3.10}$$

where y is the coordinate along the compactified extra dimension. The compactification means that

$$y \sim y + 2\pi R, \tag{3.11}$$

where R is the compactification radius. This allows us to expand the field as a Fourier series,

$$\phi(x^\mu, y) = \sum_{n=-\infty}^{\infty} \phi^{(n)}(x^\mu)\, e^{i\frac{ny}{R}}. \tag{3.12}$$

If $\phi(x^\mu, y)$ is real we have $\phi^{(n)*}(x^\mu) = \phi^{(-n)}(x^\mu)$, and we can sum from $n = 0$ instead. By inserting this expansion into equation (3.10) we get

$$\sum_{n=-\infty}^{\infty} \left(\partial_t^2 - \nabla^2 + \left(\frac{n}{R}\right)^2 + m^2\right) \phi^{(n)}(x^\mu)\, e^{i\frac{ny}{R}} = 0, \tag{3.13}$$

which means that each $\phi^{(n)}$ has to satisfy the four-dimensional Klein-Gordon equation

$$(\partial_t^2 - \nabla^2 + m_n^2)\,\phi^{(n)}(x^\mu) = 0, \tag{3.14}$$

with

$$m_n^2 = m^2 + \left(\frac{n}{R}\right)^2. \tag{3.15}$$

Each particle of mass m is therefore accompanied with a so-called *Kaluza-Klein tower* of n particle states in the four-dimensional theory with masses m_n. The fact that we have not yet seen any such particles means that the compactification radius must be small enough that the mass of the first exitation is inaccessible to our energy scales.

3.3 Other extra-dimensional theories

After the success of Kaluza and Klein of unifying gravity and electromagnetism into a single theory by introducing an extra dimension, a natural next step was to consider the possibility of unifying the other forces by introducing more dimensions. In the language of group theory, the compactified fifth dimension adds a $U(1)$ symmetry to the theory, due to translational invariance along the extra dimension. The appearence of electromagnetism is then not so surprising, since we have just included its symmetry group in a geometrical way.

The next step was then to add more dimensions in order to obtain more complicated group structures in a similar manner, such as non-Abelian groups [34]. It was then shown by Witten that in order to get the desired group structure of $SU(3) \times SU(2) \times U(1)$, one needed a minimum of 11 dimensions [35]. In addition, 11 is the highest number of dimensions which does not contain particles of spin higher than 2, which made it a reasonable choice for number of dimensions. This led to $D = 11$ supergravity, which combines Kaluza-Klein theory in 11 dimensions with the theory of supersymmetry. This theory had some problems however, for example it was difficult to include chiral fermions.

Some of these problems were solved by going to 10 dimensions instead, which led to the creation of *superstring* theory, which is still one of the few theories which could potentially provide a unified theory for all four forces of nature.

3.4 Universal extra dimensions

The theory of universal extra dimensions (UED) is essentially the standard model of particle physics in more than four spacetime dimensions, which all fields are allowed to propagate through [36]. We will here limit ourself to the case of one UED. It is important to notice that in more than four spacetime dimensions the SM is not renormalizable, so this theory should be viewed as an effective theory, valid up to some energy cutoff scale Λ. As explained previously, each of the SM fields come with a KK-tower of more massive states in four dimensions. However, the simplest method of compactifying the ED on a circle leads to a problem in the four-dimensional theory. The fifth component of a 5D vector field transforms as a scalar under 4D Lorentz transformations, which means that the zero mode of this field introduces a massless scalar field to the theory, but such fields are not observed in nature. This problem can be solved by compactifying the ED on an *orbifold* $\mathbb{S}^1/\mathbb{Z}_2$ instead of a circle, which means that in addition to the circular symmetry we also introduce a mirror symmetry between points on opposite sides of the circle, through the orbifold transformation $y \to -y$. Because of this the ED is now compactified on a half circle, $0 < y < \pi R$.

Since the Lagrangian of UED must now also be invariant under orbifold transformations, all fields in the theory must transform even or odd, $\phi(x^\mu, y) \to$

$\pm\phi(x^\mu, -y)$. Our previous expansion in Fourier modes still holds, but it now makes sense to split it into sine and cosine functions to make it explicitly odd or even. Hence, we can write

$$\phi_{\text{even}}(x^\mu, y) = \frac{1}{\sqrt{2\pi R}}\phi^{(0)}_{\text{even}}(x^\mu) + \frac{1}{\sqrt{\pi R}}\sum_{n=1}^{\infty}\phi^{(n)}_{\text{even}}\cos\left(\frac{ny}{R}\right), \tag{3.16}$$

$$\phi_{\text{odd}}(x^\mu, y) = \frac{1}{\sqrt{\pi R}}\sum_{n=1}^{\infty}\phi^{(n)}_{\text{odd}}\sin\left(\frac{ny}{R}\right). \tag{3.17}$$

Since some fields now don't have zero modes, we can avoid the problem of massless scalars by assigning appropriate orbifold transformation properties to the fields.

Our procedure is then to consider the action of the 5D theory,

$$S = \int d^4x \int_0^{2\pi R} dy\, \hat{\mathcal{L}}(x^\mu, y), \tag{3.18}$$

and perform the y-integral to eliminate the dependence on the ED, so that we end up with the action of the effective 4D theory

$$S = \int d^4x\, \mathcal{L}(x^\mu). \tag{3.19}$$

3.4.1 Gauge fields

As mentioned previously, the fifth component of vector fields must be odd under orbifold transformations. However, this can instead be achieved by demanding that the first four components transform even (which they must do to reproduce the SM at zero level) and use the requirement of gauge invariance. To see this, consider the $U(1)$ gauge transformation $A_M(x^\mu, y) \to A_M(x^\mu, y) + \partial_M\theta(x^\mu, y)$. We can then perform an orbifold projection $P_{\mathbb{Z}_2}$, and demand that it doesn't change after the gauge transformation. Using that A_μ transforms even, we get

$$\begin{aligned} P_{\mathbb{Z}_2}A_M &= P_{\mathbb{Z}_2}(A_\mu, A_5) = (A_\mu, P_{\mathbb{Z}_2}A_5) \\ &\to P_{\mathbb{Z}_2}(A_\mu + \partial_\mu\theta, A_5 + \partial_y\theta) = (A_\mu + P_{\mathbb{Z}_2}[\partial_\mu\theta], P_{\mathbb{Z}_2}A_5 + P_{\mathbb{Z}_2}[\partial_y\theta]). \end{aligned} \tag{3.20}$$

This must mean that $\partial_\mu\theta$ and therefore also θ transforms even, and thus $\partial_y\theta$ transforms odd, since $y \to -y$. To be consistent with gauge invariance, this must then mean that A_5 also transforms odd.

We can now write down the Lagrangian for the UED gauge field strength. If we limit ourself to $SU(2) \times U(1)$, the Lagrangian is

$$\hat{\mathcal{L}}_{\text{gauge}} = -\frac{1}{4}F_{MN}F^{MN} - \frac{1}{4}F^a_{MN}F^{aMN}, \tag{3.21}$$

where

$$F_{MN} = \partial_M B_N - \partial_N B_M \tag{3.22}$$

is the $U(1)$ field strength and

$$F^a_{MN} = \partial_M A^a_N - \partial_N A^a_M + \hat{g}\epsilon^{abc} A^b_M A^c_N \tag{3.23}$$

is the $SU(2)$ field strength. Apart from being in 5D, this looks identical to the gauge field Lagrangian of the SM. To calculate the 4D Lagrangian, we simply insert the odd and even expansions in equation (3.16) and (3.17) and integrate out the y-dependence. For the $U(1)$ field strength, we get

$$\begin{aligned}
\mathcal{L}^{U(1)}_{\text{gauge}} &= -\frac{1}{4}\int_0^{2\pi R} dy\, F_{MN}F^{MN} \\
&= -\frac{1}{4}\left(\partial_\mu B^{(0)}_\nu - \partial_\nu B^{(0)}_\mu\right)\left(\partial^\mu B^{(0)\nu} - \partial^\nu B^{(0)\mu}\right) \\
&\quad -\frac{1}{4}\sum_{n=1}^{\infty}\left(\partial_\mu B^{(n)}_\nu - \partial_\nu B^{(n)}_\mu\right)\left(\partial^\mu B^{(n)\nu} - \partial^\nu B^{(n)\mu}\right) \\
&\quad +\frac{1}{2}\sum_{n=1}^{\infty}\left(\partial_\mu B^{(n)}_5 + \frac{n}{R}B^{(n)}_\mu\right)\left(\partial^\mu B^{(n)}_5 + \frac{n}{R}B^{(n)\mu}\right).
\end{aligned} \tag{3.24}$$

The Lagrangian for the $SU(2)$ fields will look the same, with the addition of interaction terms. The first term in equation (3.24) is the kinetic term of the familiar $U(1)$ gauge field in the SM, while the second term is the tower of KK-states with masses n/R. There also appears to be a KK-tower of massless scalar fields $B^{(n)}_5$, but these fields can be eliminated by choosing a specific gauge. If the $B^{(n)}_\mu$ fields transform as $B^{(n)}_\mu \to B^{(n)}_\mu + \partial_\mu\left(-\frac{R}{n}B^{(n)}_5\right)$, the $B^{(n)}_5$ fields disappear and we are left with the massless $B^{(0)}_\mu$ and massive $B^{(n)}_\mu$ fields.

3.4.2 Fermions

In order to reproduce the SM at the lowest KK level, we need to get 4D *chiral* fermions for $n = 0$, meaning that the fermions are represented by left- and right-handed *Weyl spinors*. This becomes a problem in an odd number of extra dimensions, since the matrix γ^5 used to make the projection operator $P_{\text{R,L}} = 1/2(1 \pm \gamma^5)$ is part of the Clifford algebra in five dimensions, along with the four familiar gamma matrices that make up the Dirac algebra in 4D. This means that spinors in 5D are four-component Dirac spinors, and the representation is no longer reducible into two inequivalent Weyl representations.

Fortunately, our choice of orbifold projection once again comes to the rescue. By choosing appropriate transformation properties under orbifold projections, we can make sure that the fermions do not mix left and right chiral states at the lowest KK level. This gives us doublets and singlets

$$\psi_d = \frac{1}{\sqrt{2\pi R}}\psi_{d_L}^{(0)} + \frac{1}{\sqrt{\pi R}}\sum_{n=1}^{\infty}\left(\psi_{d_L}^{(n)}\cos\frac{ny}{R} + \psi_{d_R}^{(n)}\sin\frac{ny}{R}\right), \tag{3.25}$$

$$\psi_s = \frac{1}{\sqrt{2\pi R}}\psi_{s_R}^{(0)} + \frac{1}{\sqrt{\pi R}}\sum_{n=1}^{\infty}\left(\psi_{s_R}^{(n)}\cos\frac{ny}{R} + \psi_{s_L}^{(n)}\sin\frac{ny}{R}\right). \tag{3.26}$$

Note that even though the SM result is achieved at $n = 0$, all the excited KK levels still mix left and right chirality. We also get two fermions at each KK level,

$$\psi_s^{(n)} = \psi_{s_L}^{(n)} + \psi_{s_R}^{(n)}, \tag{3.27}$$

$$\psi_d^{(n)} = \psi_{d_L}^{(n)} + \psi_{d_R}^{(n)}. \tag{3.28}$$

3.4.3 Higgs fields

For completeness, we also list the scalar mass eigenstates of the 4D theory which arises from linear combinations of fields from the $U(1)$ and $SU(2)$ field strength and the complex Higgs $SU(2)$ doublet

$$\phi = \frac{1}{\sqrt{2}}\begin{pmatrix}\chi^2 + i\chi^1\\ H - i\chi^3\end{pmatrix}, \tag{3.29}$$

namely

$$a_0^{(n)} = \frac{M^{(n)}}{M_Z^{(n)}}\chi^{3(n)} + \frac{m_Z}{M_Z^{(n)}}Z_5^{(n)}, \tag{3.30}$$

$$G_0^{(n)} = \frac{m_Z}{M_Z^{(n)}}\chi^{3(n)} - \frac{M^{(n)}}{M_Z^{(n)}}Z_5^{(n)}, \tag{3.31}$$

$$a_\pm^{(n)} = \frac{M^{(n)}}{M_W^{(n)}}\chi^{\pm(n)} + \frac{m_W}{M_W^{(n)}}W_5^{\pm(n)}, \tag{3.32}$$

$$G_\pm^{(n)} = \frac{m_W}{M_W^{(n)}}\chi^{\pm(n)} - \frac{M^{(n)}}{M_W^{(n)}}W_5^{\pm(n)}, \tag{3.33}$$

where $M^{(n)} = n/R$ and

$$\chi^{\pm(n)} = \frac{1}{\sqrt{2}}(\chi^{1(n)} \mp i\chi^{2(n)}), \tag{3.34}$$

$$W_5^{\pm(n)} = \frac{1}{\sqrt{2}}(A_5^{1(n)} \mp iA_5^{2(n)}), \tag{3.35}$$

$$Z_5^{(n)} = \cos\theta_w A_5^{3(n)} - \sin\theta_w B_5^{3(n)}. \tag{3.36}$$

Thus at the lowest level, we recover the familiar scenario with one Higgs field $H^{(0)}$ and three Goldstone bosons, while for each excited KK level we have four physical fields $H^{(n)}$, $a_0^{(n)}$ and $a_\pm^{(n)}$ as well as four Goldstone bosons that generate the masses of the vector modes $A_\mu^{(n)}$, $Z_\mu^{(n)}$ and $W_\mu^{\pm(n)}$. For a complete consideration of the field content of UED as well as the interaction terms, see [30].

3.4.4 Kaluza-Klein dark matter

With all the additional particles in the UED theory, we should investigate whether some of them are viable DM candidates. If we are looking for a WIMP, the only candidate would be a particle which is stable. When the ED is compactified on an orbifold $\mathbb{S}^1/\mathbb{Z}_2$, there are some points which are invariant under the orbifold transformation $y \to -y$, namely the points $y = 0$ and $y = \pi R$. These are called the *fixpoints* of the orbifold. These fixpoints break translational invariance along the ED, which means that KK number is no longer a conserved quantity. But there is a remnant of the original symmetry left, namely translations by πR. This leads to the conserved quantity $(-1)^n$ called *KK parity*, where n is the sum of the KK numbers of all the particles involved in any interaction. Because KK parity is conserved, the lightest KK particle must be stable, and all heavier KK particles will decay down to this particle or SM particles.

The fact that no KK particles have been detected yet must mean that their masses are large compared to electroweak masses, or equivalently that the compactification scale R is small. Data from the 8 TeV run of the Large Hadron Collider have constrained the size of the ED to be $R^{-1} \gtrsim 700\,\text{TeV}$ [37]. This is a mass region which the new 13 TeV run of the LHC should be able to probe.

Because the masses of KK particles are much larger than the electroweak masses, their mass spectrum will be nearly degenerate. This makes the radiative mass corrections of UED crucial to determine the mass hierarchy of the theory. In the case of *minimal* UED (mUED), however, one assumes that these corrections don't contribute at the boundaries of the orbifold, which means that only two new parameters are introduced in the theory, namely R and Λ. In this case the lightest KK particle (LKP) is the first KK excitation of the photon, which can be approximated by the first KK level of the $U(1)$ gauge boson, $B_\mu^{(1)}$ [38]. The fact that this LKP is stable, and that it is electrically neutral and does not interact strongly makes it an excellent DM candidate. Note that the LKP is here a gauge boson, and not a Majorana fermion which is usually the case in theories with supersymmetric DM.

In order to get the correct relic density of DM, one can solve the Boltzmann equation to determine what the LKP mass should be in order to agree with the observations. In [39], it is found that the present relic density is consistent with an LKP mass of around $m_{B^{(1)}} \sim 1.3\,\text{TeV}$. This region has long been impossible

to probe by collider experiments, but it should be within reach of the LHC now running at 13 TeV [40].

Chapter 4

Gamma ray signal from dark matter

4.1 Photon-producing annihilation channels

In this section, we briefly describe the various annihilation channels of DM that produce photons. For a more complete description of gamma rays from DM, see [20].

4.1.1 Secondary photons

Since DM does not couple directly to photons, much of the gamma rays from DM come from so-called *secondary photons*, which are the decay product of other particles with a stronger coupling to DM. The DM itself decays to quarks, leptons, Higgs or gauge bosons, which in turn decay or in the case of quarks, hadronize. Most of these photons come from the process $\pi^0 \to \gamma\gamma$. Such signals result in a continuous spectrum, with a cutoff at the DM mass. Because it would simply show up as a broad excess over the background signal, it is considered a challenge to use secondary photons to detect DM.

4.1.2 Monochromatic lines

The direct annihilation of DM into photons can occur through the process $\chi\chi \to \gamma X$, where $X = \gamma, Z, H$. Because the photons don't couple directly to DM however, these processes can only happen through loop processes of order $O(\alpha_{\text{em}}^2)$, which can make them difficult to spot over the much larger background. On the other hand, the advantage with such a signal is that it is *monochromatic*, meaning that the photons are produced with the exact energy $E_\gamma = m_\chi(1 - m_X^2/4m_\chi^2)$.

4.1.3 Internal bremsstrahlung

When the annihilation product particles of DM are charged, there is a possibility that one of them radiates a photon, since they couple at $O(\alpha_{\text{em}})$. This type of radiation usually dominates at high energies. There are two types of this radiation, namely *final state radiation* and *virtual internal bremsstrahlung*, where the latter refers to photons coming from intermediate virtual particles.

4.1.4 Cascade decays

Another option is that the DM particles annihilate into two particles ϕ, each of which in turn decays into photons, either directly through $\phi \to \gamma\gamma$ or through final state radiation. If they decay directly they produce a box-shaped spectrum with a very small width, which is therefore usually indistinguishable from a line signal.

4.2 Flat spacetime

Consider a region of space with N_χ DM particles. Since particle 1 colliding with particle 2 is the same as particle 2 colliding with particle 1, the total number of available interactions is $(N_\chi^2 - N_\chi)/2$, which approaches $N_\chi^2/2$ if N_χ is large. We assume here that the DM particle is its own antiparticle. If this is not the case, like for a Dirac fermion DM particle, only half the particles are available for annihilation, and hence the number of available interactions must be multiplied by 1/2. Using the definition of the cross section σ, the rate of annihilations is then

$$W = \langle \sigma v \rangle \frac{n_\chi^2}{2} dV, \tag{4.1}$$

where $\langle \sigma v \rangle$ is the velocity-weighed cross section, dV is the infinitesimal volume of the region of space and $n_\chi = N_\chi/dV$ is the number density of the particles.

When two DM particles annihilate they can produce many different particles, but we are here only interested in the processes that produce photons. If we call the different annihilation channels f with branching ratio B_f and number of photons per energy dN_γ^f/dE_γ, the total number of photons produced per energy becomes

$$\frac{dN_\gamma}{dE_\gamma} = \frac{1}{2} \langle \sigma v \rangle \frac{\rho_\chi^2}{m_\chi^2} \sum_f B_f \frac{dN_\gamma^f}{dE_\gamma} dV, \tag{4.2}$$

where we have used $n_\chi = \rho_\chi/m_\chi$, where ρ_χ is the mass density and m_χ is the mass of the dark matter particles.

Next we choose our coordinate system to be spherical coordinates with the observer at the origin. The volume element dV is in a direction ψ, at a distance l from the origin. It spans a solid angle $d\Omega$, meaning our volume element becomes $dV = l^2 dl d\Omega$. The geometry of the situation is shown in figure 4.1. Using Gauss' theorem, the flux should be uniformly distributed in a sphere around the volume element, so at the observer the measured photon flux is

$$\frac{d\Phi_\gamma}{dE_\gamma} = \frac{dN_\gamma/dE_\gamma}{4\pi l^2} = \frac{1}{8\pi}\langle\sigma v\rangle \frac{\rho_\chi^2}{m_\chi^2} \sum_f B_f \frac{dN_\gamma^f}{dE_\gamma} dl d\Omega. \tag{4.3}$$

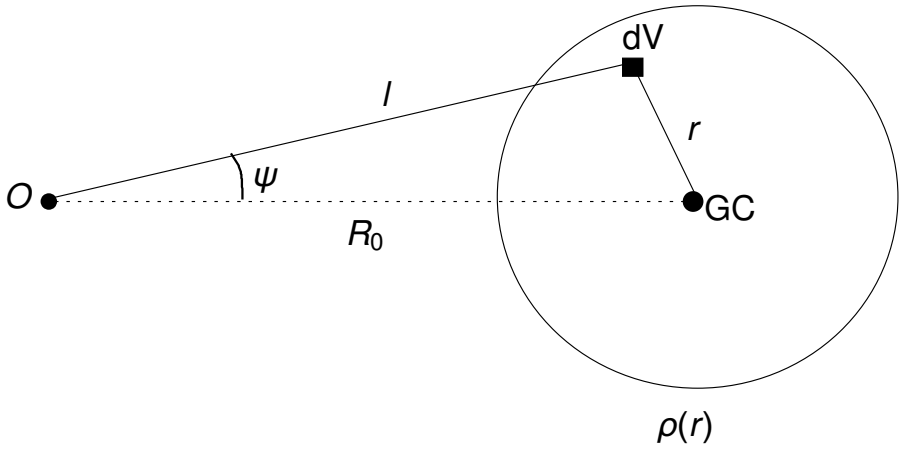

Figure 4.1: Sketch of the geometric situation. The observer at O is observing the galaxy at an angle ψ away from the galactic center GC. He recieves gamma rays from photons annihilating in the volume element dV, at a distance l away from the observer and a distance r from the galactic center. In order to obtain the total gamma ray flux one must integrate the DM density $\rho(r)$ along the line of sight l, in principle from zero to infinity. The geometry is symmetric with respect to rotations around the line R_0 connecting the observer to the galactic center. Since the density is a function of r, we need to relate this variable to l and ψ in order to perform the integral.

Thus for a continuous DM distribution, we get the total flux by integrating

along the line of sight. Finally, our expression for the measured differential gamma ray flux from dark matter annihilations in a direction ψ becomes

$$\frac{d\Phi_\gamma}{d\Omega dE_\gamma}(E_\gamma, \psi) = \frac{1}{8\pi} \int_{\text{l.o.s.}} dl(\psi) \rho_\chi^2(\mathbf{r}) \left[\frac{\langle \sigma v \rangle}{m_\chi^2} \sum B_f \frac{dN_\gamma^f}{dE_\gamma} \right]. \tag{4.4}$$

In this equation, the terms in the parenthesis contain the particle physics information. It is usually assumed that the DM particles in our galaxy annihilate with vanishing velocity, which means that the particle physics part can be pulled outside the integral. The remaining part is then the astrophysical factor,

$$J(\psi) = \int_{\text{l.o.s.}} dl(\psi) \rho_\chi^2(\mathbf{r}), \tag{4.5}$$

containing the spatial information about the signal.

It is however often more useful to consider the integrated flux over some solid angle $\Delta\Omega$, corresponding to the region of observation. We then average our $J(\psi)$ over the region $\Delta\Omega$,

$$\bar{J}(\Delta\Omega) = \frac{1}{\Delta\Omega} \int_{\Delta\Omega} d\Omega. \tag{4.6}$$

If our region of observation is a cone centered on the galactic center, then our solid angle becomes

$$\Delta\Omega = 2\pi \int_0^{\psi_{\max}} d\psi \, \sin\psi. \tag{4.7}$$

While this assumption that the particles annihilate at rest is usually warrented when considering DM in our galaxy, there are situations where this may no longer be the case, such as for DM annihilating close to a black hole. Considering the full velocity dependence could then enhance the signal, especially in the case of KK dark matter [6].

As an example, we can calculate the J factor for a NFW profile, using `Mathematica` to compute the integral numerically. We insert the expression for r as a function of l and ψ, using the law of cosines:

$$r = \sqrt{l^2 + R_0^2 - 2lR_0 \cos\psi}, \tag{4.8}$$

where R_0 is the distance from the sun to the galactic center. In figure 4.2, we show the function $J(\psi)$ calculated for the different profiles presented in section 2.3. Here we see that the result is greatly dependent on the shape of the DM halo, and whether or not it is enhanced by density spikes. The result for the straight NFW profile with $\gamma' = 1$ also seems to agree with the result from [25].

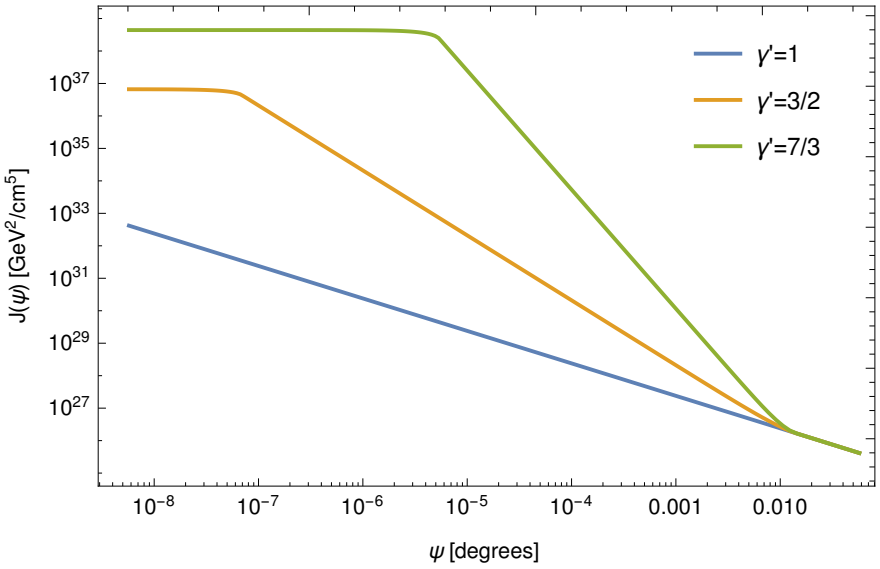

Figure 4.2: The integral $J(\psi)$ which contains the square of the DM density integrated along the line of sight. We here show $J(\psi)$ for three different density profiles, where the lowest curve is just a NFW profile, while the other two are enhanced by density spikes by susbstituting $\gamma \to \gamma'$ in the profile $\rho^{-\gamma}$. The curves stabilize when our viewing angle reaches the density plateau, as the DM density no longer increases closer to the black hole.

4.3 Curved spacetime

The equation for the recieved gamma ray flux from dark matter annihilations in our galaxy, equation 4.4, is only valid when we can neglect the curvature of spacetime, which is fine for most applications. But as we know, at the center of our Milky Way galaxy there is a supermassive black hole, with a mass of 4 million solar masses [41]. For the photons coming from DM annihilations from the innermost regions of the galaxy, the black hole will alter their trajectory and energy, because of the spacetime curvature. It is intirely possible that this effect is strong enough to significantly influence the gamma ray flux measured here on earth, which is why it is of interest to investigate these effects.

In this section, we take into account the path the photons take when travelling through curved space. In the original derivation of the equation in Minkowski spacetime, we assumed that the photons produced from annihilations in the galactic DM halo travelled in a straight line from the point where they were created to the observer, and therefore integrated along that line. In order to take into account curvature however, we should instead integrate along the geodesic curves of the photons, which are not necessarily straight lines.

To model the black hole at the galactic center, we will assume a Schwarzschild spacetime, which is discussed in Appendix B. For a more complete consideration

of this metric and other topics in general relativity, see for example Carroll's textbook *Spacetime and geometry: An introduction to general relativity* [42]. The geodesics of photons in the Schwarzschild spacetime are described completely by the variables r and ϕ, where r is the distance from the center and ϕ is the angle in the x-y plane. the variables are parametrized by λ, and the resulting geodesic equations are

$$\frac{dr}{d\lambda} = \sqrt{E^2 - \left(1 - \frac{R_s}{r}\right)\frac{L^2}{r^2}}, \tag{4.9}$$

$$\frac{d^2\phi}{d\lambda^2} + \frac{2}{r}\frac{d\phi}{d\lambda}\frac{dr}{d\lambda} = 0, \tag{4.10}$$

where $E = (1 - R_s/r)dt/d\lambda$ and $L = r^2 d\phi/d\lambda$ are constants of motion. Since the Schwarzschild geodesics are time-symmetric, we can solve the equations as geodesics starting at the observer at $r(0) = R_0$ and $\phi(0) = 0$, with $\dot{\phi}(0) = \dot{\phi}_0$, where the dot means differentiation with respect to λ. This last initial condition is a function of the angle ψ with which we observe the galaxy.

We can find expressions for the constants E and L by evaluating them at the observer at $r = R_0$, where $R_s \ll R_0$. To lowest order, we then get

$$E = \frac{dt}{d\lambda} = E_\gamma, \tag{4.11}$$

which by definition is the photon energy. We can relate L to the observation angle ψ by considering the three-vector

$$\frac{dx^i}{d\lambda} = \dot{r}\,\hat{e}_r + r\dot{\phi}\,\hat{e}_\phi, \tag{4.12}$$

where $\hat{e}_r$ and $\hat{e}_\phi$ are unit vectors in the r and ϕ direction, respectively. at the location of the observer, the components of equation 4.11 are related to ψ by the trigonometric relation

$$R_0\,\dot{\phi}(0) = \sqrt{\dot{r}(0)^2 + R_0^2\,\dot{\phi}(0)^2}\,\sin\psi. \tag{4.13}$$

By inserting equation 4.9 evaluated at $\lambda = 0$ and only keeping terms to lowest order in R_s/R_0, we get

$$L = R_0 E_\gamma \sin\psi, \quad \dot{\phi}(0) = \frac{E_\gamma}{R_0}\sin\psi. \tag{4.14}$$

By inserting these expressions for E and L in equation 4.9, we get our equation for r in terms of E_γ and ψ:

$$\frac{dr}{d\lambda} = E_\gamma\sqrt{1 - \left(1 - \frac{R_s}{r}\right)\left(\frac{R_0}{r}\right)^2\sin^2\psi}. \tag{4.15}$$

A solution to equations 4.15 and 4.10 can be seen in figure 4.3, where we have plotted the photon geodesics for four slightly different values of ψ, ranging from 2×10^{-9} to 9×10^{-9} degrees. When viewed as photons falling toward the black hole, we see that the three geodesics passing closest eventually fall in through the event horizon, while the outermost geodesic carries enough energy to escape after orbiting the black hole once. The geodesic curves are the same for photons travelling in the opposite direction however, in which case the three closest geodesics correspond to photons being produced close to the black hole, with enough energy to escape and reach the observer at the point $r = R_0$ along the x axis. It is worth noting that the photons being produced at the event horizon would have an infinite redshift, and they would therefore not be detectable in practice. The last geodesic describes photons coming from infinitely far away, and passing by the black hole in such a way that their trajectories get redirected just right to hit the observer. However, we should remember that the DM density far away from the black hole drops quickly, therefore the majority of photons contributing to the observed flux will come from annihilations along the geodesics close to the black hole.

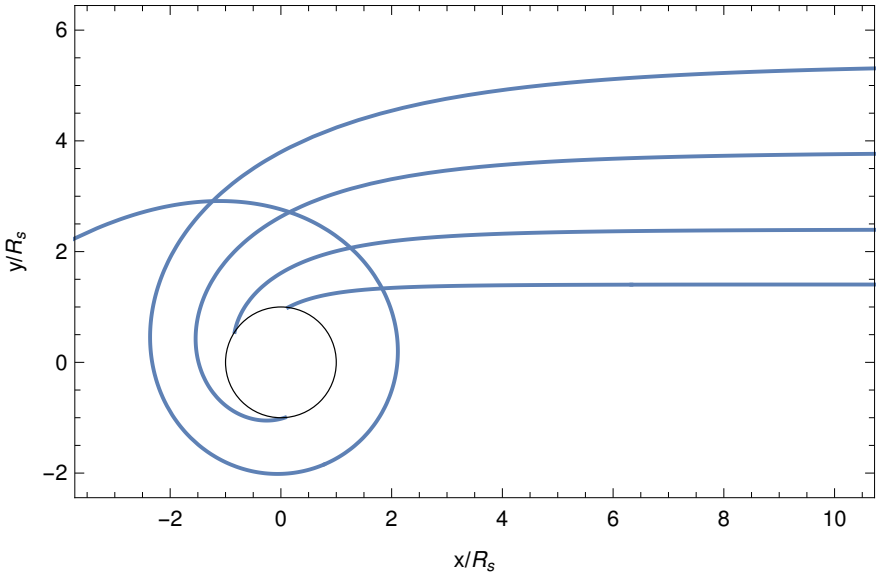

Figure 4.3: A selection of geodesics close to the event horizon of a black hole. Since the Schwarzschild equations are time symmetric, we can think of these both as photons falling into the black hole or as photons being created close to the event horizon. In the latter case, which is what corresponds to our situation, all the geodesics coincide at an observer at the point $x = R_0$, $y = 0$. There are two kinds of geodesics seen here, the ones that impact the Schwarzschild radius of the black hole and the ones that slingshot around it and continues to infinity. The geodesics shown here correspond to observation angles ranging from 2×10^{-9} to 9×10^{-9} degrees.

Integrating along geodesics instead of the straight line of sight, our equation 4.4 changes to

$$\frac{d\Phi_\gamma}{d\Omega dE_\gamma}(E_\gamma,\psi) = \frac{1}{8\pi}\int_{\text{l.o.s.}} dl(\psi,\lambda)\rho_\chi^2(\mathbf{r})\left[\frac{\langle\sigma v\rangle}{m_\chi^2}\sum B_f\frac{dN_\gamma^f}{dE_\gamma}\right], \tag{4.16}$$

where $dl(\psi,\lambda)$ is the line element along the geodesic curve corresponding to the observation angle ψ. This line element can be written in terms of r and ϕ through the relation

$$dl(\psi,\lambda) = \sqrt{r^2 d\phi^2 + dr^2}, \tag{4.17}$$

from which we can extract a factor $d\lambda$ to get

$$dl(\psi,\lambda) = \sqrt{r^2\left(\frac{d\phi}{d\lambda}\right)^2 + \left(\frac{dr}{d\lambda}\right)^2}\,d\lambda. \tag{4.18}$$

Substituting $d\phi/d\lambda$ with L and inserting equation 4.9 for $dr/d\lambda$, we get the line element

$$dl(\psi,\lambda) = E_\gamma\sqrt{1+\frac{R_s R_0^2}{r^3}\sin^2\psi}. \tag{4.19}$$

We can now calculate the J factor as we did in section 4.2, but this time the integral is

$$J(\psi) = \int dl(\psi,\lambda)\rho^2(r). \tag{4.20}$$

4.4 Gravitational redshift

The next step in generalizing equation 4.4 is to consider the frequency shift of the measured photons which occurs because they come from further down a strong gravitational well. In order to do this, we need to realize that the energy E_γ of the photons in equation 4.4 are no longer the same when they are emitted as when they are observed, which means that we need to alter our equation to

$$\frac{d\Phi_\gamma}{dE_\gamma}(E_\gamma,\psi) = \frac{1}{8\pi}\frac{1}{\Delta\Omega}\int_{\Delta\Omega} d\Omega\int_{\text{l.o.s.}} dl(\psi,\lambda)\rho_\chi^2(\mathbf{r})\left[\frac{\langle\sigma v\rangle}{m_\chi^2}\sum B_f\frac{dN_\gamma^f}{dE'_\gamma}\right], \tag{4.21}$$

where E'_γ is the energy of the emitted photon. This is then the generalized form of equation 4.4, taking into account both the gravitational redshift and the curved

paths of the photons, where we have now integrated over $\Delta\Omega$ to consider the total flux from photons from within an angle ψ of the galactic center.

In order to solve this equation, we thus need to relate E_γ to E'_γ. This can be found by using the formula for the gravitational redshift in Schwarzschild coordinates, which is deduced in appendix B. This gives the relation

$$E'_\gamma = \frac{E_\gamma}{\sqrt{1 - \frac{R_s}{r}}}. \tag{4.22}$$

The simplest case to consider is monochromatic lines from the process $\chi\chi \to \gamma\gamma$, meaning that each photon produced has an energy $E'_\gamma = \sqrt{s}/2$, where s is the center of mass-energy squared. If we also assume that the DM particles annihilate at rest, the annihilation cross section $\langle\sigma v\rangle$ becomes constant and can be moved outside the integral, while the energy of each photon becomes simply the mass of the DM particles, $E'_\gamma = m_\chi$. The number of photons produced becomes

$$\sum B_f \frac{dN^f_\gamma}{dE'_\gamma} = 2\delta(E'_\gamma - m_\chi). \tag{4.23}$$

Since we want to integrate over λ, we use the following identity for the delta function:

$$\delta(f(\lambda)) = \frac{\delta(\lambda - \lambda_0)}{|f'(\lambda_0)|}, \tag{4.24}$$

where $f(\lambda) = E'_\gamma(r(\lambda)) - m_\chi$, λ_0 is the zero point for $f(\lambda)$ and $f'(\lambda_0)$ is the derivative of f with respect to λ at the point $\lambda = \lambda_0$. The only zero point of f is when $E'_\gamma(r(\lambda_0)) = m_\chi$, which gives us r at the zero point

$$r(\lambda_0) = \frac{R_s}{1 - E^2_\gamma/m^2_\chi}. \tag{4.25}$$

We can then perform the integral over λ using the delta function.

Using all of this and changing to the dimensionless variable $x = E_\gamma/m_\chi$, the equation 4.21 becomes

$$\frac{d\Phi_\gamma}{dx} = \frac{R_s}{2\pi}\frac{\langle\sigma v\rangle}{m^2_\chi}\rho^2\left(\frac{R_s}{1-x^2}\right)\frac{x^2}{(1-x^2)^2}\frac{1}{1-\cos\psi}\int_0^{\psi_{\max}} g(\psi', x)\sin\psi' d\psi', \tag{4.26}$$

where

$$g(\psi', x) = \sqrt{\frac{1 + R^2_0/R^2_s\,(1-x^2)^3\sin^2\psi'}{1 - R^2_0/R^2_s\,x^2(1-x^2)^2\sin^2\psi'}}, \tag{4.27}$$

and

$$\psi_{\max} = \text{Min}\left[\psi,\, \sin^{-1}\left(\frac{R_s/R_0}{x(1-x^2)}\right)\right]. \tag{4.28}$$

This choice of integration variable comes from the fact that for a given value of x, there is a maximum value $\psi_{\max}$ from which photons are recieved. This is the angle where the expression $g(\psi', x)$ is no longer well defined, because the expression in the denominator becomes negative.

Chapter 5

Results and discussion

5.1 $J(\psi)$ in Schwarzschild coordinates

The J-factor in Schwarzschild coordinates as described in section 4.3 is calculated numerically using `Mathematica`, and the result is shown in figure 5.1. For all calculations we have used a black hole mass of 4.31×10^6 solar masses corresponding to a Schwarzschild radius of $R_s = 4.1 \times 10^{-7}$ pc, and $R_0 = 8.33$ kpc [43]. The DM profile is here chosen to have $\gamma' = 3/2$.

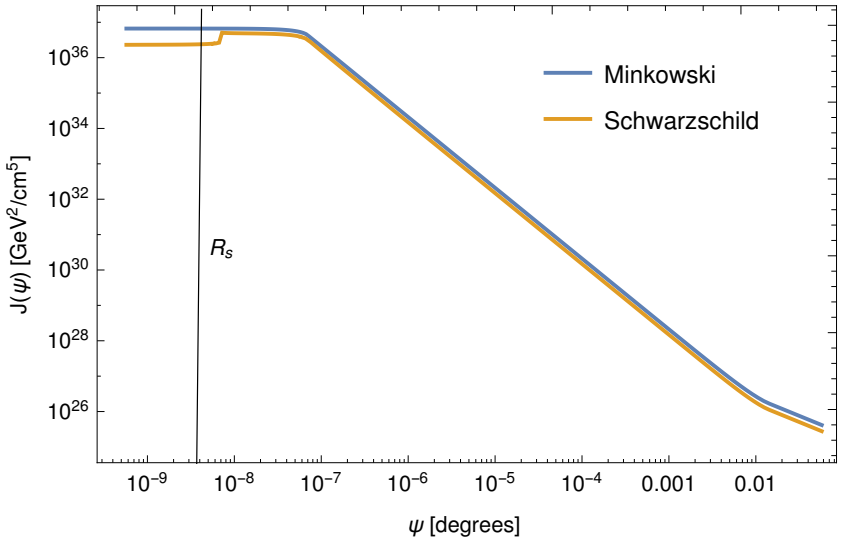

Figure 5.1: $J(\psi)$ calculated in Schwarzschild coordinates compared to the same expression in Minkowski space. The vertical line inserted indicates the angle at which a straight line from the observer comes within the Schwarzschild radius of the black hole. For both curves the DM profile with $\gamma' = 3/2$ is used. The Schwarzschild radius used is $R_s = 4.1 \times 10^{-7}$ pc, and the distance to the observer is $R_0 = 8.33$ kpc.

The difference between the Minkowski and Schwarzschild solution seen for large angles ψ appears to be a numerical error, as we would expect the two solutions to be equal when we are viewing the galaxy far away from the black hole at the center. When taking this into account, the two graphs are more or less identical until we get to an angle equivalent to a radius from the center just a little larger than the Schwarzschild radius. Here the J-factor for Schwarzschild drops, which is because at this angle photons can no longer reach us by travelling around the black hole, or in other words, the geodesics we integrate along now impacts the black hole instead of curving around it. This means that the amount of photons able to reach us are significantly reduced.

As the observation angle gets smaller, $J(\psi)$ for both graphs seem to become constant. This is to be expected, since as the angle goes to zero the geodesics are practically straight lines toward the center of the black hole. Note that the vertical line only indicates the angle at which a straight line drawn from the observer passes closest to the black hole at a radius equal to the Schwarzschild radius.

While we do see a difference in the Minkowski and Schwarzschild solution, this difference is only apparent for extremely small angles, and even then the difference is probably too small to be observable. More importantly, the current angular resolution of detectors is nowhere near the necessary resolution to resolve these differences. The HESS collaboration has for example recently surveyed gamma rays from the galactic center [44], but only at observation angles down to 0.3°. Part of the reason why smalles angles are challenging is due to the large uncertainties in the DM density profile at these small distances, as we have discussed previously in this thesis. There is however the possibility that with a better understanding of the behaviour of DM at the galactic center, as well as with better detectors, we will eventually be able to observe the influence of the black hole on the photons, as we have described.

5.2 The spectral signal

In figure 5.2, we see the expected flux of gamma rays for an observation angle from the galactic center of $\psi = 5.7 \times 10^{-9}\,^\circ$. We have set the DM annihilation cross section to be $\langle \sigma v \rangle = 10^{-25}\text{cm}^3/\text{s}$, and the DM mass to $m_\chi = 1$ TeV. Since we assume the particles annihilate at rest and therefore the photons are produced with $E'_\gamma = m_\chi$, we see that most of the particles are redshifted by a factor of about $\Delta x = 0.1$.

Figure 5.3 for a slightly larger value of $\psi = 5.7 \times 10^{-8}\,^\circ$ is more interesting, as it shows a slight bump at $x = 0.05$, but unfortunately we cannot rule out that this is due to a numerical error. It is however an intriguing possibility that the slight excess of strongly redshifted photons are due to the unstable orbit at $r = 3R_s/2$, where the photons can orbit the black hole multiple times before

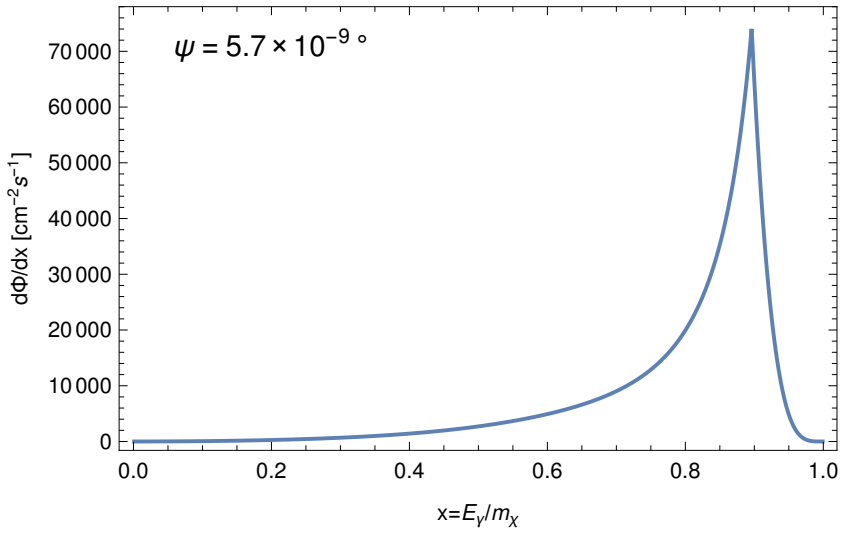

Figure 5.2: The gamma ray flux from the galactic center within a cone of angular radius $\psi = 5.7 \times 10^{-9}\,^\circ$. The DM particles are assumed to annihilate at rest, and the annihilation cross section and DM mass are set to $10^{-25}\text{cm}^3/\text{s}$ and 1 TeV, respectively.

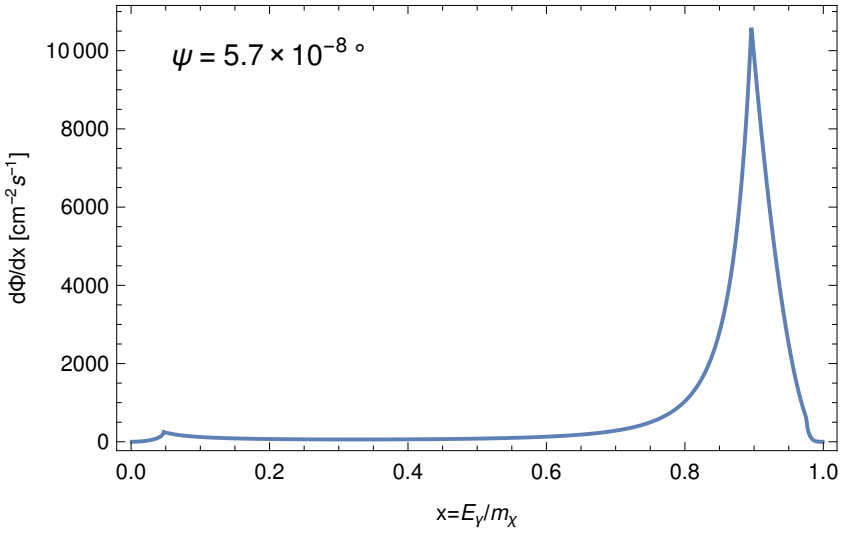

Figure 5.3: The gamma ray flux from the galactic center within a cone of angular radius $\psi = 5.7 \times 10^{-8}\,^\circ$. The DM particles are assumed to annihilate at rest, and the annihilation cross section and DM mass are set to $10^{-25}\text{cm}^3/\text{s}$ and 1 TeV, respectively. The slight bump at $x = 0.05$ is possibly a numerical error, but it could also be due to extremely redshifted photons originating from close to the black hole.

escaping and reaching the observer. If there is a buildup of photons at this radius, we should expect to see an excess in the flux at the corresponding redshift. Note also that there seems to be a slight relative increase of photons with x close to one in this figure compared to figure 5.2, which we would expect as photons from a slightly larger angle don't come as close to the black hole, and are therefore not as redshifted.

Our suspicion that the small bump in figure 5.3 is due to numerical errors is strengthened when considering figure 5.4, where we show the photon flux for a larger angle of $\psi = 5.7\,^\circ$. At such a large angle we don't expect to see a large flux of photons at all, and as we see the dominant contribution still comes from the photons close to the black hole, redshifted by $\Delta x = 0.1$. We are however unable to make physical sense of the steep increase close to $x = 0$, and if there was a contribution from the stable orbit at $r = 3R_s/2$ we would expect a bump for the same value of x as in figure 5.3. We therefore think this comes from a numerical error. If the result for the slight redshift of the majority of the photons holds however, it could potentially be detectable with present day detectors. The challenge is then to see this signal over the background from the galactic center, which is still not completely understood.

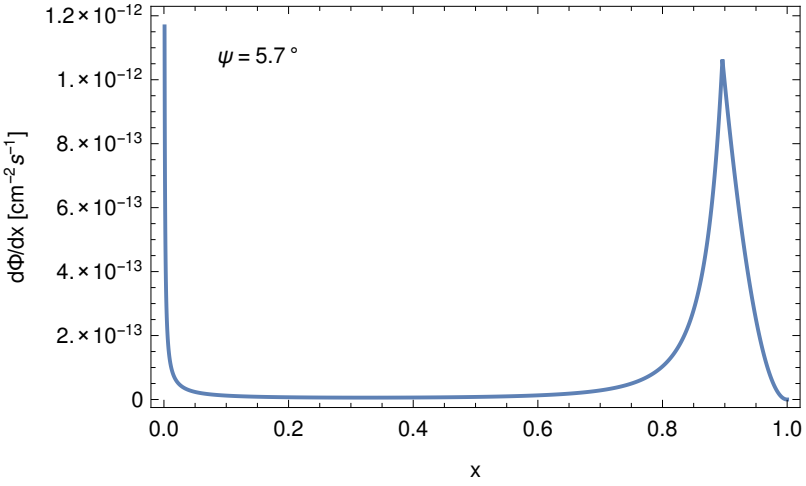

Figure 5.4: The gamma ray flux from the galactic center within a cone of angular radius $\psi = 5.7 \times 10^{-8}\,^\circ$. The DM particles are assumed to annihilate at rest, and the annihilation cross section and DM mass are set to $10^{-25}\text{cm}^3/\text{s}$ and 1 TeV, respectively. The steep increase at x close to zero strengthens our suspicion that this feature is due to numerical error.

Finally, it is important to realize that our assumption of annihilation at the resonance $E'_\gamma = m_\chi$ is probably an oversimplification. While the DM particles in the galaxy at large can usually be assumed to annihilate at rest, the situation is probably very different in the vicinity of a black hole. In addition to adding

a conventional Doppler shift to the energy E'_γ due to the particles falling toward the black hole, it also means that the cross section $\langle \sigma v \rangle$ is no longer independent of the velocity of the DM particles, and can therefore not be taken outside the integral over $dl(\psi, \lambda)$. This completly changes the expression for the number of photons produced from annihilations, as the velocity distribution of the particles would also have to be taken into account. It would be interesting to see such a calculation done, as it probably would yield more realistic results. Unfortunately, we were not able to do so in this thesis due to time constraints.

Chapter 6

Conclusions

In this thesis, we have investigated the effects of general relativity on gamma rays from annihilating DM. The motivation was that for certain DM models such as KK DM, the inclusion of the velocity dependent annihilation cross section could produce striking features making it easier to identify a signal. In [6], some investigation of the gravitational and Doppler reshift for KK DM had been done, but it seemed no consideration of other effects from general relativity on such a signal existed. We therefore wanted to find out how this signal would change when also things like the photon geodesics were taken into account.

In Section 4.2, we started by deriving the standard expression for gamma ray flux in Minkowski space, and applying it on a possible DM density profile in the region close to a black hole.

Then we proceeded to alter this expression to include relativistic effects, by taking into account both the curved paths of the photons instead of simply integrating along a straight line, and that the photons would no longer have the same energy when observed as when they were created, due to the gravitational redshift. We used expressions derived in the Schwarzschild spacetime to model the black hole at the galactic center.

We then proceeded to apply these expressions to an example, first by calculating the factor $J(\psi)$ in Schwarzschild coordinates and comparing to the equivalent expression in Minkowski space. While there was a small difference for observational angles corresponding to photons coming from annihilations close to the event horizon of the black hole, these differences are very small when one considers the large uncertainties in the DM density profile for small radii. In addition, the observational angles at which the relativistic effects became apparent were much smaller than the angular resolution of current gamma ray detectors.

Next, we considered the case of DM particles annihilating at rest in the Schwarzschild spacetime, meaning that all photons were created at resonance where the energy of the photons are exactly equal to the DM mass. We found that these photons were redshifted by $\Delta x = 0.1$ for an observational angle of $\psi = 5.7 \times 10^{-9}\,^\circ$. For a larger angle of $\psi = 5.7 \times 10^{-8}\,^\circ$, there seemed to be

an increase in photon flux for photons redshifted down to $x = 0.05$, which could be due to the unstable orbit located at $3R_s/2$ where the photons could build up before travelling to the observer. We were however unable to determine whether or not this was the case, and it remains a possibility that this increase is due to numerical error. For a larger angle of $\psi = 5.7\,^\circ$ the dominant contribution still comes from photons close to the black hole that are redshifted by $\Delta x = 0.1$, but a steep increase close to $x = 0$ strengthens our suspicion that this feature and the slight bump for $\psi = 5.7 \times 10^{-8}\,^\circ$ are due to numerical errors. if the redshift of $\Delta x = 0.1$ for the other photons is correct it might be detectable however, but such a signal could be difficult to filter out due to the many poorly understood background processes at the galactic center.

It was originally our intention to also consider the case where the DM particles have non-vanishing velocity, as is likely when considering the DM profile close to the black hole. We were however unable to do this due to lack of time. In such a scenario the DM particles would get an additional Doppler shift due to their motion toward the black hole, and it would also have altered the signal because the velocity dependent cross section would have to be included in the integral.

While the conclusion is that our results would probably be undetectable with current data, it is hopefully just a matter of time before the density profile of the inner regions of the galaxy and the background processes are known well enough to actually see such effects originating from general relativity.

Appendix A

The geodesic equation

The geodesic equation is the equation for the shortest path between two points in a (potentially) curved spacetime. If the curve is paremetrized by a parameter λ, then the length of the curve is given by the integral

$$S = \int ds(\lambda), \tag{A.1}$$

where ds is the infinitesimal line element of the curve and the integral is taken over the entire curve. Using that $ds^2 = g_{\mu\nu}dx^\mu dx^\nu$, we can write the integral as

$$S = \int \sqrt{g_{\mu\nu}dx^\mu dx^\nu} = \int \sqrt{g_{\mu\nu}\dot{x}^\mu \dot{x}^\nu}d\lambda \equiv \int L\, d\lambda, \tag{A.2}$$

where $\dot{x}^\mu \equiv \frac{dx^\mu}{d\lambda}$. In the rest of the calculation, we will assume that the metric $g_{\mu\nu}$ is only a function of the coordinates x^μ, not its derivatives.

Our task is then to minimize the length of this curve, meaning

$$\delta S = \int \delta\sqrt{g_{\mu\nu}\dot{x}^\mu \dot{x}^\nu}d\lambda = 0. \tag{A.3}$$

However, in order to simplify calculations we note that minimizing the integral over L is in this case the same as minimizing the integral over L^2, so we will instead consider the expression

$$\int \delta(g_{\mu\nu}\dot{x}^\mu \dot{x}^\nu)\, d\lambda = 0. \tag{A.4}$$

The problem then reduces to the Euler-Lagrange equations,

$$\frac{d}{d\lambda}\left(\frac{\partial W}{\partial \dot{x}^\beta}\right) - \frac{\partial W}{\partial x^\beta} = 0, \tag{A.5}$$

where $W = L^2 = g_{\mu\nu}\dot{x^\mu}\dot{x^\nu}$.

We then have

$$\frac{\partial W}{\partial x^\beta} = g_{\mu\nu,\beta}\dot{x^\mu}\dot{x^\nu}, \tag{A.6}$$

where $,\beta$ denotes partial differentiation with respect to β.

$$\frac{\partial W}{\partial \dot{x}^\beta} = g_{\mu\nu}(\delta^\mu_\beta \dot{x^\nu} + \dot{x^\mu}\delta^\nu_\beta) = 2g_{\beta\mu}\dot{x^\mu}. \tag{A.7}$$

$$\frac{d}{d\lambda}\left(\frac{\partial W}{\partial \dot{x}^\beta}\right) = 2\left(\frac{dx^\nu}{d\lambda}\frac{\partial}{\partial x^\nu}g_{\beta\mu}\dot{x^\mu} + g_{\beta\mu}\ddot{x^\mu}\right) = 2\left(g_{\beta\mu,\nu}\dot{x^\mu}\dot{x^\nu} + g_{\beta\mu}\ddot{x^\mu}\right), \tag{A.8}$$

where we have used the chain rule in the first term.

Inserting these expressions into the Euler-Lagrange equations and multiplying by $g^{\alpha\beta}/2$, we get

$$\ddot{x}^\alpha + \frac{1}{2}g^{\alpha\beta}\left(2g_{\beta\mu,\nu}\dot{x^\mu}\dot{x^\nu} - g_{\mu\nu,\beta}\dot{x^\mu}\dot{x^\nu}\right) = 0. \tag{A.9}$$

The first term in the paranthesis is symmetric in exchanging μ and ν, and can be rewritten

$$2g_{\beta\mu,\nu}\dot{x^\mu}\dot{x^\nu} = g_{\beta\mu,\nu}\dot{x^\mu}\dot{x^\nu} + g_{\beta\nu,\mu}\dot{x^\mu}\dot{x^\nu}. \tag{A.10}$$

Using this, our final expression becomes

$$\ddot{x}^\alpha + \Gamma^\alpha_{\mu\nu}\dot{x}^\mu\dot{x}^\nu = 0, \tag{A.11}$$

where $\Gamma^\alpha_{\mu\nu}$ are the Christoffel symbols,

$$\Gamma^\alpha_{\mu\nu} = \frac{1}{2}g^{\alpha\beta}\left(g_{\beta\mu,\nu} + g_{\beta\nu,\mu} - g_{\mu\nu,\beta}\right). \tag{A.12}$$

This is the usual expression for the geodesic equation.

Appendix B

The Schwarzschild solution

The Schwarzschild line element is

$$ds^2 = -\left(1 - \frac{R_s}{r}\right) dt^2 + \frac{dr^2}{1 - \frac{R_s}{r}} + r^2(d\theta^2 + \sin^2\theta d\phi^2), \tag{B.1}$$

where $R_s = 2GM$ is the Schwarzschild radius. The non-zero Christoffel symbols are

$$\begin{aligned}
&\Gamma^r_{tt} = \frac{GM}{r^3}(r - R_s), && \Gamma^r_{rr} = -\frac{GM}{r(r - R_s)}, && \Gamma^t_{tr} = \frac{GM}{r(r - R_s)}, \\
&\Gamma^\theta_{r\theta} = \frac{1}{r}, && \Gamma^r_{\theta\theta} = -(r - R_s), && \Gamma^\phi_{r\phi} = \frac{1}{r}, \\
&\Gamma^r_{\phi\phi} = -(r - R_s)\sin^2\theta, && \Gamma^\theta_{\phi\phi} = -\sin\theta\cos\theta, && \Gamma^\phi_{\theta\phi} = \frac{\cos\theta}{\sin\theta}.
\end{aligned} \tag{B.2}$$

Using that $ds^2 = g_{\mu\nu}dx^\mu dx^\nu$, we can write the Lagrangian

$$L = \frac{1}{2} g_{\mu\nu} \frac{dx^\mu}{d\lambda} \frac{dx^\nu}{d\lambda} = -\frac{1}{2}\left(1 - \frac{R_s}{r}\right) \dot{t}^2 + \frac{1}{2} \frac{\dot{r}^2}{1 - \frac{R_s}{r}} + \frac{1}{2} r^2(\dot{\theta}^2 + \sin^2\theta\, \dot{\phi}^2), \tag{B.3}$$

where the dot indicates differentiation with respect to λ. We notice that our Lagrangian does not depend explicitly on t or ϕ, and hence these are cyclic coordinates. The corresponding conserved quantities are

$$p_t = \frac{\partial L}{\partial \dot{t}} = \left(1 - \frac{R_s}{r}\right) \dot{t} \equiv -E, \tag{B.4}$$

$$p_\phi = \frac{\partial L}{\partial \dot{\phi}} = r^2 \sin^2\theta\, \dot{\phi} \equiv L. \tag{B.5}$$

Using that the four-velocity squared for photons is zero, we get the equation

$$g_{\mu\nu}\frac{dx^\mu}{d\lambda}\frac{dx^\nu}{d\lambda} = -\frac{1}{2}\left(1-\frac{R_s}{r}\right)\dot{t}^2 + \frac{1}{2}\frac{\dot{r}^2}{1-\frac{R_s}{r}} + \frac{1}{2}r^2(\dot{\theta}^2+\sin^2\theta\,\dot{\phi}^2) = 0. \tag{B.6}$$

We can now substitute E and L for the coordinates $\dot{t}$ and $\dot{\phi}$:

$$-\frac{E^2}{1-\frac{R_s}{r}} + \frac{\dot{r}^2}{1-\frac{R_s}{r}} + r^2\dot{\theta}^2 + \frac{L^2}{r^2\sin^2\theta} = 0. \tag{B.7}$$

We can simplify this equation further by investigating the geodesic equation for θ. Setting the index $\mu = 2$ and inserting Christoffel symbols, we get

$$\frac{d^2\theta}{d\lambda^2} + \frac{2}{r}\frac{d\theta}{d\lambda}\frac{dr}{d\lambda} - \sin\theta\cos\theta\left(\frac{d\theta}{d\lambda}\right)^2 = 0. \tag{B.8}$$

This can be rewritten as

$$\frac{d}{d\lambda}\left(r^2\dot{\theta}\right) - r^2\sin\theta\cos\theta\,\dot{\phi}^2 = 0, \tag{B.9}$$

and after substituting L for $\dot{\phi}$ it becomes

$$\frac{d}{d\lambda}\left(r^2\dot{\theta}\right) = \frac{L^2\cos\theta}{r^2\sin\theta}. \tag{B.10}$$

If we multiply both sides with $r^2\dot{\theta}$, we can do the integral over λ to get

$$\left(r^2\dot{\theta}\right)^2 = k - \left(\frac{L}{\sin\theta}\right)^2, \tag{B.11}$$

where k is a constant of integration.

We can always choose our coordinates such that the light moves in the equatorial plane at $t = 0$, namely with

$$\theta(t=0) = \frac{\pi}{2}, \quad \dot{\theta}(t=0) = 0, \tag{B.12}$$

which means that we can determine the constant k to be L^2, and the equation becomes

$$\left(r^2\dot{\theta}\right)^2 = L^2\left(1-\frac{1}{\sin^2\theta}\right). \tag{B.13}$$

For this equation to hold, however, the expression

$$\left(1-\frac{1}{\sin^2\theta}\right) \tag{B.14}$$

must always be positive, and the only way to make this happen is if $\theta = \frac{\pi}{2}$ for all t. Thus, our equation B.7 does not depend on θ, and it now becomes

$$-E^2 + \dot{r}^2 + \left(1 - \frac{R_s}{r}\right)\frac{L^2}{r^2} = 0. \tag{B.15}$$

This is then our equation for r. The equations for ϕ and t can be obtained from the geodesic equation, and read

$$\ddot{\phi} + \frac{2}{r}\dot{\phi}\,\dot{r} = 0, \tag{B.16}$$

$$\ddot{t} + \frac{R_s}{r(r - R_s)}\dot{r}\,\dot{t} = 0. \tag{B.17}$$

We can also find the expression for the gravitational redshift in Schwarzschild coordinates by considering an observer with four-velocity U^μ. If the observer is at rest, this implies $U^i = 0$. The four-velocity must satisfy the equation $g_{\mu\nu}U^\mu U^\nu = -1$, and since $g_{00} = -(1 - R_s/r)$ we get

$$U^0 = \left(1 - \frac{R_s}{r}\right)^{-1/2}. \tag{B.18}$$

Thus, for a photon travelling along a geodesic $x^\mu(\lambda)$, the energy is

$$E' = -g_{\mu\nu}U^\mu \frac{dx^\nu}{d\lambda}, \tag{B.19}$$

which becomes

$$E' = \left(1 - \frac{R_s}{r}\right)^{1/2}\frac{dt}{d\lambda} = \left(1 - \frac{R_s}{r}\right)^{-1/2} E, \tag{B.20}$$

where E is the constant determined in equation B.4.

Bibliography

[1] Planck Collaboration, "Planck 2015 results. XIII. Cosmological parameters", arXiv:1502.01589.

[2] M. Taoso, G. Bertone, and A. Masiero, "Dark Matter Candidates: A Ten-Point Test", *JCAP* **0803** (2008) 022, doi:10.1088/1475-7516/2008/03/022, arXiv:0711.4996.

[3] G. Jungman, M. Kamionkowski, and K. Griest, "Supersymmetric dark matter", *Phys. Rept.* **267** (1996) 195–373, doi:10.1016/0370-1573(95)00058-5, arXiv:hep-ph/9506380.

[4] A. N. Baushev, "Dark matter annihilation in the gravitational field of a black hole", *Int. J. Mod. Phys.* **D18** (2009) 1195, doi:10.1142/S0218271809014509, arXiv:0805.0124.

[5] H.-C. Cheng, J. L. Feng, and K. T. Matchev, "Kaluza-Klein dark matter", *Phys. Rev. Lett.* **89** (2002) 211301, doi:10.1103/PhysRevLett.89.211301, arXiv:hep-ph/0207125.

[6] C. Arina et al., "Enhanced Line Signals from Annihilating Kaluza-Klein Dark Matter", *Phys. Rev.* **D90** (2014), no. 8, 083506, doi:10.1103/PhysRevD.90.083506, arXiv:1409.0007.

[7] F. Zwicky, "Die Rotverschiebung von extragalaktischen Nebeln", *Helv. Phys. Acta* **6** (1933) 110–127.

[8] V. C. Rubin and W. K. Ford, Jr., "Rotation of the Andromeda Nebula from a Spectroscopic Survey of Emission Regions", *Astrophys. J.* **159** (1970) 379–403, doi:10.1086/150317.

[9] D. Clowe et al., "A direct empirical proof of the existence of dark matter", *Astrophys. J.* **648** (2006) L109–L113, doi:10.1086/508162, arXiv:astro-ph/0608407.

[10] S. W. Randall et al., "Constraints on the Self-Interaction Cross-Section of Dark Matter from Numerical Simulations of the Merging Galaxy Cluster

1E 0657-56", *Astrophys. J.* **679** (2008) 1173–1180, doi:10.1086/587859, arXiv:0704.0261.

[11] B. D. Wandeltet al., "Selfinteracting dark matter", in *Sources and detection of dark matter and dark energy in the universe. Proceedings, 4th International Symposium, DM 2000, Marina del Rey, USA, February 23-25, 2000*, pp. 263–274. 2000. arXiv:astro-ph/0006344.

[12] M. Milgrom, "A Modification of the Newtonian dynamics as a possible alternative to the hidden mass hypothesis", *Astrophys. J.* **270** (1983) 365–370, doi:10.1086/161130.

[13] G. Bertone, D. Hooper, and J. Silk, "Particle dark matter: Evidence, candidates and constraints", *Phys. Rept.* **405** (2005) 279–390, doi:10.1016/j.physrep.2004.08.031, arXiv:hep-ph/0404175.

[14] T. Marrodán Undagoitia and L. Rauch, "Dark matter direct-detection experiments", *J. Phys.* **G43** (2016), no. 1, 013001, doi:10.1088/0954-3899/43/1/013001, arXiv:1509.08767.

[15] R. Bernabei et al., "Final model independent result of DAMA/LIBRA-phase1", *Eur. Phys. J.* **C73** (2013) 2648, doi:10.1140/epjc/s10052-013-2648-7, arXiv:1308.5109.

[16] T. Bringmann et al., "Fermi LAT Search for Internal Bremsstrahlung Signatures from Dark Matter Annihilation", *JCAP* **1207** (2012) 054, doi:10.1088/1475-7516/2012/07/054, arXiv:1203.1312.

[17] Fermi-LAT Collaboration, "Search for gamma-ray spectral lines with the Fermi large area telescope and dark matter implications", *Phys. Rev.* **D88** (2013) 082002, doi:10.1103/PhysRevD.88.082002, arXiv:1305.5597.

[18] IceCube Collaboration, "Improved limits on dark matter annihilation in the Sun with the 79-string IceCube detector and implications for supersymmetry", arXiv:1601.00653.

[19] PAMELA Collaboration, "An anomalous positron abundance in cosmic rays with energies 1.5-100 GeV", *Nature* **458** (2009) 607–609, doi:10.1038/nature07942, arXiv:0810.4995.

[20] T. Bringmann and C. Weniger, "Gamma Ray Signals from Dark Matter: Concepts, Status and Prospects", *Phys. Dark Univ.* **1** (2012) 194–217, doi:10.1016/j.dark.2012.10.005, arXiv:1208.5481.

[21] R. Catena and P. Ullio, "A novel determination of the local dark matter density", *JCAP* **1008** (2010) 004, doi:10.1088/1475-7516/2010/08/004, arXiv:0907.0018.

[22] J. F. Navarro, C. S. Frenk, and S. D. M. White, "A Universal density profile from hierarchical clustering", *Astrophys. J.* **490** (1997) 493–508, doi:10.1086/304888, arXiv:astro-ph/9611107.

[23] J. F. Navarro, V. R. Eke, and C. S. Frenk, "The cores of dwarf galaxy halos", *Mon. Not. Roy. Astron. Soc.* **283** (1996) L72–L78, doi:10.1093/mnras/283.3.L72, arXiv:astro-ph/9610187.

[24] A. W. Graham et al., "Empirical models for Dark Matter Halos. I. Nonparametric Construction of Density Profiles and Comparison with Parametric Models", *Astron. J.* **132** (2006) 2685–2700, doi:10.1086/508988, arXiv:astro-ph/0509417.

[25] M. Cirelli et al., "PPPC 4 DM ID: A Poor Particle Physicist Cookbook for Dark Matter Indirect Detection", *JCAP* **1103** (2011) 051, doi:10.1088/1475-7516/2012/10/E01,10.1088/1475-7516/2011/03/051, arXiv:1012.4515. [Erratum: JCAP1210,E01(2012)].

[26] G. Bertone and D. Merritt, "Dark matter dynamics and indirect detection", *Mod. Phys. Lett.* **A20** (2005) 1021, doi:10.1142/S0217732305017391, arXiv:astro-ph/0504422.

[27] G. Bertone and D. Merritt, "Time-dependent models for dark matter at the Galactic Center", *Phys. Rev.* **D72** (2005) 103502, doi:10.1103/PhysRevD.72.103502, arXiv:astro-ph/0501555.

[28] O. Y. Gnedin and J. R. Primack, "Dark Matter Profile in the Galactic Center", *Phys. Rev. Lett.* **93** (2004) 061302, doi:10.1103/PhysRevLett.93.061302, arXiv:astro-ph/0308385.

[29] J. M. Overduin and P. S. Wesson, "Kaluza-Klein gravity", *Phys. Rept.* **283** (1997) 303–380, doi:10.1016/S0370-1573(96)00046-4, arXiv:gr-qc/9805018.

[30] T. Bringmann, "Cosmological aspects of universal extra dimensions". PhD thesis, Stockholm U., 2005.

[31] T. Kaluza, "On the Problem of Unity in Physics", *Sitzungsber. Preuss. Akad. Wiss. Berlin (Math. Phys.)* **1921** (1921) 966–972.

[32] P. Jordan, "Erweiterung der projektiven Relativitätstheorie", *Annalen der Physik* **436** (1947), no. 4-5, 219–228, doi:10.1002/andp.19474360409.

[33] O. Klein, "Quantum Theory and Five-Dimensional Theory of Relativity. (In German and English)", *Z. Phys.* **37** (1926) 895–906, doi:10.1007/BF01397481. [Surveys High Energ. Phys.5,241(1986)].

[34] B. S. DeWitt, "Dynamical theory of groups and fields", *Conf. Proc.* **C630701** (1964) 585–820. [Les Houches Lect. Notes13,585(1964)].

[35] E. Witten, "Search for a Realistic Kaluza-Klein Theory", *Nucl. Phys.* **B186** (1981) 412, doi:10.1016/0550-3213(81)90021-3.

[36] T. Appelquist, H.-C. Cheng, and B. A. Dobrescu, "Bounds on universal extra dimensions", *Phys. Rev.* **D64** (2001) 035002, doi:10.1103/PhysRevD.64.035002, arXiv:hep-ph/0012100.

[37] T. Kakuda et al., "Phenomenological constraints on universal extra dimensions at LHC and electroweak precision test", arXiv:1304.6362.

[38] G. Servant and T. M. P. Tait, "Is the lightest Kaluza-Klein particle a viable dark matter candidate?", *Nucl. Phys.* **B650** (2003) 391–419, doi:10.1016/S0550-3213(02)01012-X, arXiv:hep-ph/0206071.

[39] G. Belanger, M. Kakizaki, and A. Pukhov, "Dark matter in UED: The Role of the second KK level", *JCAP* **1102** (2011) 009, doi:10.1088/1475-7516/2011/02/009, arXiv:1012.2577.

[40] A. Belyaev et al., "Discovering Minimal Universal Extra Dimensions (MUED) at the LHC", *JHEP* **06** (2013) 080, doi:10.1007/JHEP06(2013)080, arXiv:1212.4858.

[41] A. M. Ghez et al., "Measuring Distance and Properties of the Milky Way's Central Supermassive Black Hole with Stellar Orbits", *Astrophys. J.* **689** (2008) 1044–1062, doi:10.1086/592738, arXiv:0808.2870.

[42] S. M. Carroll, "Spacetime and geometry: An introduction to general relativity". 2004.

[43] S. Gillessen et al., "Monitoring stellar orbits around the Massive Black Hole in the Galactic Center", *Astrophys. J.* **692** (2009) 1075–1109, doi:10.1088/0004-637X/692/2/1075, arXiv:0810.4674.

[44] HESS Collaboration, "Search for a Dark Matter annihilation signal from the Galactic Center halo with H.E.S.S", *Phys. Rev. Lett.* **106** (2011) 161301, doi:10.1103/PhysRevLett.106.161301, arXiv:1103.3266.